NAVAL POSTGRADUATE SCHOOL

MONTEREY, CALIFORNIA

THESIS

GRANULAR MATERIAL RESPONSE TO DYNAMIC SHOCK COMPRESSION: A STUDY OF SIO_2 IN THE FORM OF SAND AND SODA LIME GLASS BEADS

by

James R. Santymire

June 2011

Thesis Advisor:	Jose Sinibaldi
Co-Advisor	Robert Hixson

Approved for public release; distribution is unlimited

THIS PAGE INTENTIONALLY LEFT BLANK

REPORT DOCUMENTATION PAGE			Form Approved OMB No. 0704-0188
Public reporting burden for this collection of information is estimated to average 1 hour per response, including the time for reviewing instruction, searching existing data sources, gathering and maintaining the data needed, and completing and reviewing the collection of information. Send comments regarding this burden estimate or any other aspect of this collection of information, including suggestions for reducing this burden, to Washington headquarters Services, Directorate for Information Operations and Reports, 1215 Jefferson Davis Highway, Suite 1204, Arlington, VA 22202-4302, and to the Office of Management and Budget, Paperwork Reduction Project (0704-0188) Washington DC 20503.			
1. AGENCY USE ONLY ***(Leave blank)***	**2. REPORT DATE** June 2011	**3. REPORT TYPE AND DATES COVERED** Master's Thesis	
4. TITLE AND SUBTITLE Granular Material Response to Dynamic Shock Compression: A Study of SiO_2 in the Form of Sand and Soda Lime Glass Beads		**5. FUNDING NUMBERS**	
6. AUTHOR(S) James R. Santymire			
7. PERFORMING ORGANIZATION NAME(S) AND ADDRESS(ES) Naval Postgraduate School Monterey, CA 93943-5000		**8. PERFORMING ORGANIZATION REPORT NUMBER**	
9. SPONSORING /MONITORING AGENCY NAME(S) AND ADDRESS(ES) N/A		**10. SPONSORING/MONITORING AGENCY REPORT NUMBER**	
11. SUPPLEMENTARY NOTES The views expressed in this thesis are those of the author and do not reflect the official policy or position of the Department of Defense or the U.S. Government. IRB Protocol number. N/A			
12a. DISTRIBUTION / AVAILABILITY STATEMENT Approved for public release; distribution is unlimited		**12b. DISTRIBUTION CODE**	

13. ABSTRACT (maximum 200 words)

There has been increased interest in the dynamic behavior of sand throughout scientific and engineering communities due, mainly, to its damaging mechanisms against armored military vehicles upon sudden acceleration from buried improvised explosive devices. NASA is also interested in the properties of sand as a stimulant for powdered planetary materials. This thesis focused on developing the experimental techniques to successfully measure its dynamic response to shock impacts.

However, sand has widely variant compositions based on its geographic location and environmental conditions making it difficult to repeat experimental results. This research has examined the use of widely available commercial 'technical sand' composed of uniform sized, nearly spherical soda lime glass beads as a viable alternative for modeling sand. This allows for the repetition of experimental results independent of geographical location, thus providing a basis to better correlate and compare data between various focus areas of research.

The objective of this thesis was to establish/develop the required experimental setup and procedures that will account for the inherent difficulty of experimentation with this material due to their solid and fluid like properties. Additionally, the first several Hugoniot data points were measured for this technical sand at pressures below one GPa.

14. SUBJECT TERMS Sand, Soda lime, glass beads, Hugoniot, shock physics			**15. NUMBER OF PAGES** 105
			16. PRICE CODE
17. SECURITY CLASSIFICATION OF REPORT Unclassified	**18. SECURITY CLASSIFICATION OF THIS PAGE** Unclassified	**19. SECURITY CLASSIFICATION OF ABSTRACT** Unclassified	**20. LIMITATION OF ABSTRACT** UU

NSN 7540-01-280-5500 Standard Form 298 (Rev. 2-89)
Prescribed by ANSI Std. 239-18

THIS PAGE INTENTIONALLY LEFT BLANK

Approved for public release; distribution is unlimited

GRANULAR MATERIAL RESPONSE TO DYNAMIC SHOCK COMPRESSION: A STUDY OF SIO_2 IN THE FORM OF SAND AND SODA LIME GLASS BEADS

James R. Santymire
Lieutenant, United States Navy
B.S., United States Naval Academy, 2003

Submitted in partial fulfillment of the
requirements for the degree of

MASTER OF SCIENCE IN APPLIED PHYSICS

from the

NAVAL POSTGRADUATE SCHOOL
June 2011

Author: James R. Santymire

Approved by: Professor Jose Sinibaldi
Thesis Advisor

Professor Robert Hixson
Co-Advisor

Professor Andres Larraza
Chair, Department of Physics

THIS PAGE INTENTIONALLY LEFT BLANK

ABSTRACT

There has been increased interest in the dynamic behavior of sand throughout scientific and engineering communities due, mainly, to its damaging mechanisms against armored military vehicles upon sudden acceleration from buried improvised explosive devices. NASA is also interested in the properties of sand as a stimulant for powdered planetary materials. This thesis focused on developing the experimental techniques to successfully measure its dynamic response to shock impacts.

However, sand has widely variant compositions based on its geographic location and environmental conditions making it difficult to repeat experimental results. This research has examined the use of widely available commercial 'technical sand' composed of uniform sized, nearly spherical soda lime glass beads as a viable alternative for modeling sand. This allows for the repetition of experimental results independent of geographical location, thus providing a basis to better correlate and compare data between various focus areas of research.

The objective of this thesis was to establish/develop the required experimental setup and procedures that will account for the inherent difficulty of experimentation with this material due to their solid and fluid like properties. Additionally, the first several Hugoniot data points were measured for this technical sand at pressures below one GPa.

THIS PAGE INTENTIONALLY LEFT BLANK

TABLE OF CONTENTS

LIST OF FIGURES

LIST OF TABLES

THIS PAGE INTENTIONALLY LEFT BLANK

LIST OF ACRONYMS AND ABBREVIATIONS

AL6061	Aluminum alloy 6061
Cu	Copper
OFHC	Oxygen Free High Conductivity
EFP	Explosively Formed Penetrator
IED	Improvised Explosive Device
HEL	Hugoniot Elastic Limit
ISP	Institute for Shock Physics
LANL	Los Alamos National Lab
LLNL	Lawrence Livermore National Lab
SNL	Sandia National Lab
NPS	Naval Postgraduate School
mm	Millimeter, or one thousandth of a meter
μm	Micrometer, or one millionth of a meter
nm	Nanometer, or one billionth of a meter
mrad	Milliradians, or one thousandth of a radian
ms	Milliseconds, or one thousandth of a second
μs	Microseconds, or one millionth of a second
ns	Nanoseconds, or one billionth of a second
g/cc	Gram per cubic centimeter
GPa	Gigapascals, one billion pascals of pressure to force per unit area
VISAR	Velocity Interferometer System for Any Reflector

THIS PAGE INTENTIONALLY LEFT BLANK

ACKNOWLEDGMENTS

First and foremost, I must express my deepest gratitude to my amazing bride and family whose loving support has allowed me to undertake and complete this endeavor.

Next, I would like to thank my thesis advisors, Prof. Jose Sinibaldi and Prof. Robert Hixson, for their support. Their expertise has helped me to understand the various intricacies contained within this complicated field. Without their guidance, I would not have achieved the goal of completing this thesis.

The support of others was also instrumental in the successful completion of this research. A special thanks to Prof. Nancy Haegel, George Jaksha, Sam Barone and Chanman Park for their aid.

THIS PAGE INTENTIONALLY LEFT BLANK

I. INTRODUCTION

A. GOALS AND OBJECTIVES

The goal of this research is to improve the understanding of the dynamic response of sand. In order to further this understanding, this research examines the use of widely available commercial *technical sand* composed of uniformed sized, nearly spherical soda lime glass beads as a viable alternative for modeling sand. This will require the establishment and development of an experimental setup and procedure that will account for the inherent difficulty of experimentation with granular and porous media due to their solid and fluid-like properties. Additionally, this research measures the first several data points for the Hugoniot of this technical sand at pressures below one GPa.

B. BACKGROUND

1. Granular and Porous Materials

a. Interest in Granular and Porous Media

Granular and porous media are of growing interest in a number of fields of study throughout the scientific community. Of these materials, sand is receiving a significant amount of attention due to the wide range of environments in which it is found and the many ways that it is used as a component in products that are produced.

Sand is of growing interest to those studying armor concepts as they need a better model and understanding of how sand interacts with and is affected by buried improvised explosive devices (IEDs) shown in Figure 1, and explosively formed penetrators (EFPs) shown in Figure 2.

Figure 1. IED device discovered in 2005 in eastern Baghdad

Figure 2. EFP with concave copper cap

When these devices are detonated, the shock waves interact with the sand, causing the sand to compact and become additional projectiles that cause damage to vehicles and personnel in the vicinity of the explosion, as shown in Figure 3.

Figure 3. HUMVEE damaged by an EFP

NASA is also interested in the properties of sand as a stimulant for powdered planetary materials. Impact processes involving such materials are ubiquitous, and played a major role in planet formation and dynamics. Research into granular materials provides a better understanding of how these particulates interact with their surroundings on the surfaces of neighboring celestial bodies. The focus is on how the granular particles found on the surface of the moon and Mars are affected by impact from meteors and other objects that become trapped in these bodies' gravitational wells or are otherwise sent on an impact trajectory. The surfaces of the moon and Mars have a partial surface layer of material that share similar characteristics with sand.

In 2009, NASA conducted an impact experiment on the moon in an attempt to find water. NASA's Lunar CRater Observation and Sensing Satellite (LCROSS) and Lunar Reconnaissance Orbiter (LRO) were successful in collecting data from the LCROSS impact allowing NASA to identify pure water ice grains along with a myriad of other compounds. In order to plan this attempt it was imperative to know how much force would be needed to cause sufficient penetration into the lunar crust and the expected characteristics of the debris cloud that would be formed, shown in Figure 4 [1].

Having a better understanding of how sand is affected by impact will allow for more accurate models to be created and adapted to more accurately simulate the dynamic response of these granular materials.

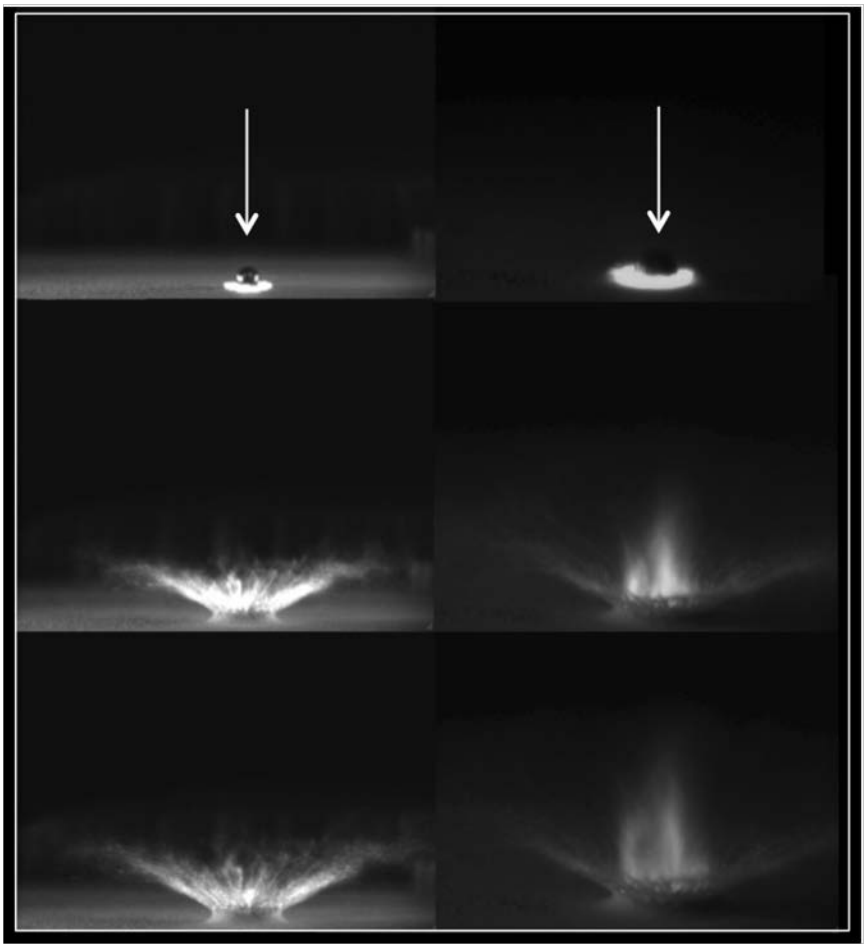

Figure 4. After [1]. Experiments at the Ames Vertical Gun Range helped researchers understand the LCROSS impact. Image credit: Brown University/Peter H. Schultz and Brendan Hermalyn, NASA/Ames Vertical Gun Range. Separate all from/after with period, or else it looks like a run-on sentence

Geologists, seismologists and the construction industry have long been interested in the shock properties of sand. The geological community studies the properties of sand in a wide variety of locations in order to determine how it is affected by shock waves that travel through it due to earthquakes and other man-made shocks.

The construction industry is likewise interested in its properties for this reason and because it is a critical component in the making of concrete.

b. Inherent Difficulty in Determining Shock Properties

Granular and porous materials are some of the most difficult materials to study and to determine their shock properties. Granular materials, such as sand, are comprised of many small particulates that combine to make a whole body of material. On the microscopic level, we can break sand down and discuss individual particulates that make up the whole. However, we are unable to study the shock properties of these individual particulates and, were we able to, the shock properties of each individual particulate would vary due to differences in elemental makeup and a lone particulate would not accurately represent the particulates taken as a whole body.

When these particulates are combined into a whole body or mass contained in a fixed volume space, they undergo a certain level of compaction when dynamically compacted. This compaction reduces the volume of air surrounding each particulate. These voids of air are part of the reason why it is difficult for the shock properties of these materials to be determined. For granular materials, the compaction process is made somewhat more difficult as porous materials demonstrate both fluid like and solid like behaviors. The study of sand is further complicated due its varying composition and the diversity of the physical characteristics of the particulates based on their geographic location.

2. Physical Properties of Sand

Sand is a naturally occurring granular material with a wide variety of compositions based on geographical location. The most common types of sand are primarily composed of silicon dioxide or SiO_2 in the form of quartz. The remaining materials that compose sand are dependent on local mineral sources and surrounding elements. The size and shape of the individual particles are affected by the environment in which the sand is located and the weathering experienced. Individual grain sizes of sand range from 0.02 mm up to 4.76 mm depending on the standard used as shown in

Figure 5 [2]. Figures 6 and 7 show a sampling of sand found in various geographic locations representing some of the most common perceptions of sand. Figure 8 shows a detailed image of sand used in shock impact experiments at Sandia National Laboratories.

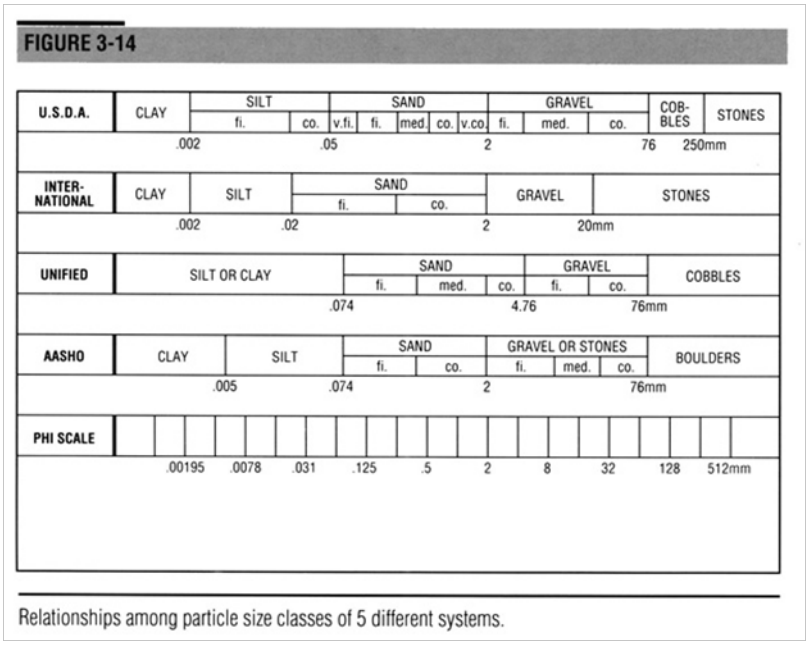

Figure 5. From [2] Relationship among particle size classes of 5 different systems

Figure 6. Sand from Pismo Beach, CA

Figure 7. Sand dunes in the Sahara desert in Libya. Image Credit: Luca Galuzzi.

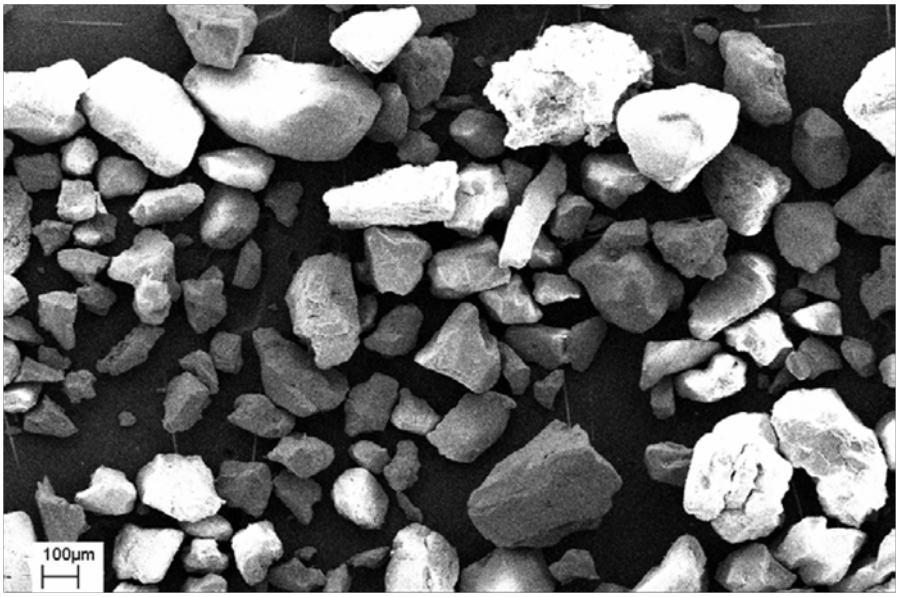

Figure 8. From [3] SEM image of untested sand powder. Image credit: Sandia National Laboratories

3. Physical Properties of Technical Sand

In order to create a standard base material for future experimentation and modeling, it is necessary to choose a material that allows for repetition of experimental results independent of geographical location. This requires that commercially available technical sand be used. The technical sand used for experimentation was a glass oxide bead found commercially and that is used for sand blasting. The beads are made from

soda lime glass with a chemical composition of 74% SiO_2, 13% Na_2O, 10.5% CaO, 1.3% Al_2O_3, 0.3% K_2O, 0.2% SO_3, 0.2% MgO, 0.04% Fe_2O_3, and 0.01% TiO_2. The grain size ranged from 177 μm to 250 μm, sieve sizes 60-80 or military specification seven. The particles were found to be primarily spherical with occasional particles found that were fused together in various configurations providing dispersion among the sample representative of coarser particles. The average measured density of non-compacted technical sand was 1.536 g/cc or approximately 60.9% of full density for soda lime glass. Figure 9 provides detailed imaging of a sampling of the technical sand.

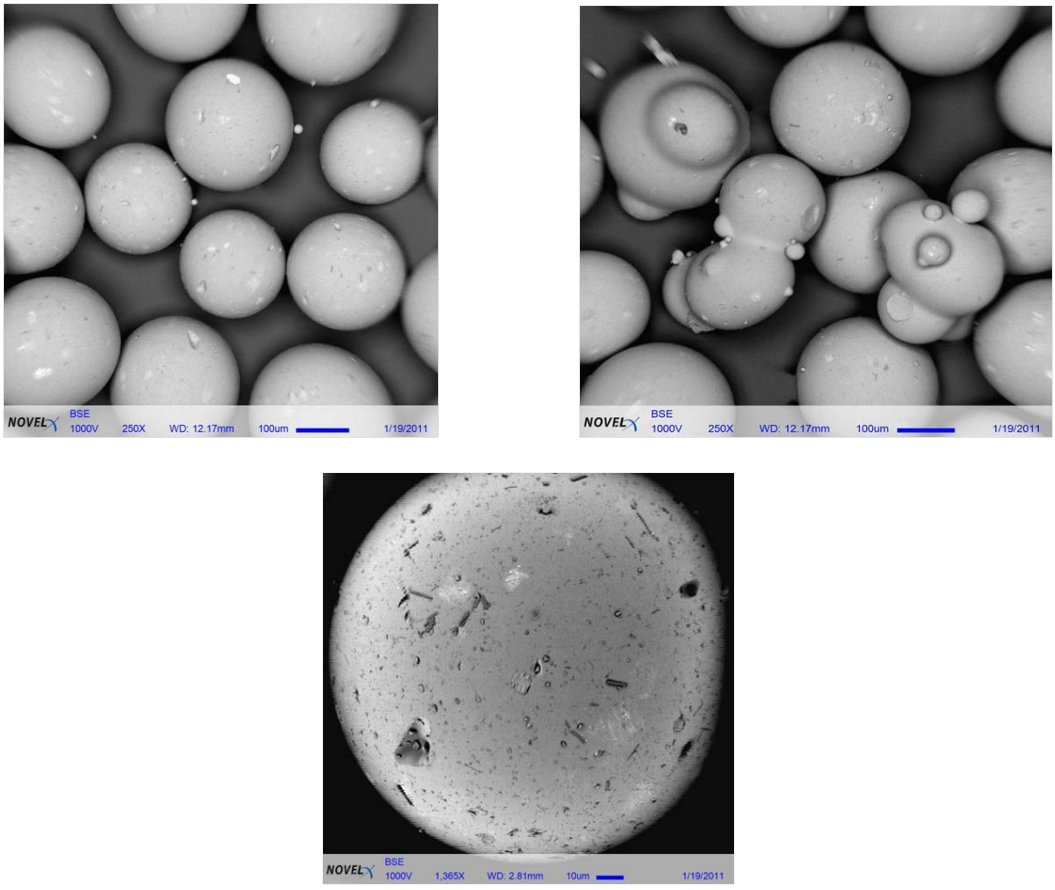

Figure 9. SEM image of glass oxide beads.
Image credit: DR Nancy Haegel, Naval Postgraduate School.

C. RESEARCH APPROACH

Due to the challenges that this project presents, a careful and concise approach will be used to achieve the end goals and recommendations. This research begins with an overview of current shock theory based on years of previous development and will use fundamental shock compression techniques that have also been vetted through years of use. This research will focus primarily on developing the process for future experimentation of granular and porous media at the Naval Postgraduate School, obtaining initial Hugoniot data points for technical sand and to help better understand the dynamic response of the sand.

THIS PAGE INTENTIONALLY LEFT BLANK

II. EXPERIMENTAL METHODS

A. INTRODUCTION TO SHOCK PHYSICS

1. Static Elastic-Plastic Theory

The object of this research is to develop a process by which the shock properties of granular and porous media are able to be determined via experimentation. In order to dynamically characterize a material, some theory about the dynamic response of materials in general must be understood. All materials have a dynamic response to impulse loading from a dynamic event based on the inherent properties that govern them. In order to better understand these events, we will use and adapt a simple suite of dynamic experiments. First, however, an understanding of how materials respond to static loading conditions must be understood. Certain elements of elastic theory are relevant to this research and will be reviewed.

When a material is loaded under stress, it responds by contracting or expanding based on whether the stress applied places the material in compression or tension respectively. Therefore, the material strain is proportional to the stress loading. This is shown in Figure 10 for a material under uniaxial stress conditions.

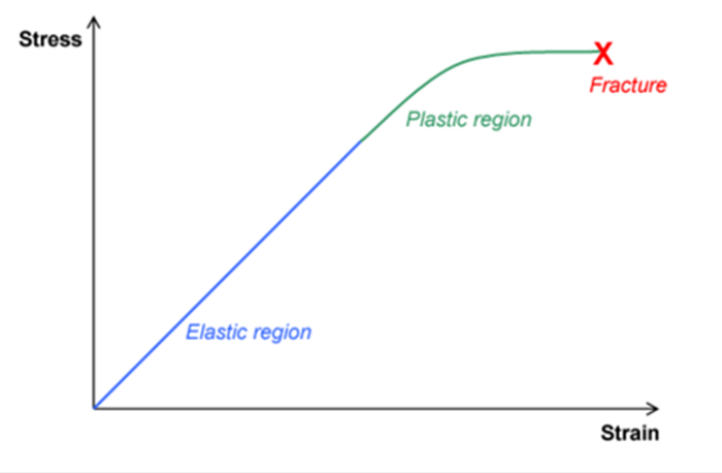

Figure 10. Diagram of stress strain curve for linear elastic materials

The relationship between stress and strain in the linear elastic region is defined by Young's Modulus, E, and is the ratio of stress over strain:

$$E = \frac{\sigma_x}{\varepsilon_x}$$

Young's modulus is a fundamental modulus for states of uniaxial stress and is often referred to as the 'elastic modulus.' When a material reaches the limit for linear response it transitions from elastic to plastic deformation. The strain that occurs as a result of plastic deformation is unrecoverable and therefore, not elastic. The region of plastic deformation is important in this research due to the porous attributes of the technical sand. When sand experiences a high velocity impact or a strong shock is propagated through it, it undergoes compaction, and given adequate force it is plastically deformed. However, since it takes a considerable amount of force to reach a state of full compaction and fuse these particulates into a uniform solid, the elastic deformation regime is also important for impact problems. In the elastic regime, stress and strain are related though the general constitutive relation:

$$\begin{bmatrix} \sigma_{xx} \\ \sigma_{yy} \\ \sigma_{zz} \\ \sigma_{yz} \\ \sigma_{zx} \\ \sigma_{xy} \end{bmatrix} = \begin{bmatrix} C_{11} & C_{12} & C_{13} & C_{14} & C_{15} & C_{16} \\ C_{21} & C_{22} & C_{23} & C_{24} & C_{25} & C_{26} \\ C_{31} & C_{32} & C_{33} & C_{34} & C_{35} & C_{36} \\ C_{41} & C_{42} & C_{43} & C_{44} & C_{45} & C_{46} \\ C_{51} & C_{52} & C_{53} & C_{54} & C_{55} & C_{56} \\ C_{61} & C_{62} & C_{63} & C_{64} & C_{65} & C_{66} \end{bmatrix} \begin{bmatrix} \varepsilon_{xx} \\ \varepsilon_{yy} \\ \varepsilon_{zz} \\ \varepsilon_{yz} \\ \varepsilon_{zx} \\ \varepsilon_{xy} \end{bmatrix}$$

For isotropic materials this simplifies due to symmetry:

$$\begin{bmatrix} \sigma_{xx} \\ \sigma_{yy} \\ \sigma_{zz} \\ \sigma_{yz} \\ \sigma_{zx} \\ \sigma_{xy} \end{bmatrix} = \begin{bmatrix} \lambda+2\mu & \lambda & \lambda & 0 & 0 & 0 \\ \lambda & \lambda+2\mu & \lambda & 0 & 0 & 0 \\ \lambda & \lambda & \lambda+2\mu & 0 & 0 & 0 \\ 0 & 0 & 0 & \mu & 0 & 0 \\ 0 & 0 & 0 & 0 & \mu & 0 \\ 0 & 0 & 0 & 0 & 0 & \mu \end{bmatrix} \begin{bmatrix} \varepsilon_{xx} \\ \varepsilon_{yy} \\ \varepsilon_{zz} \\ \varepsilon_{yz} \\ \varepsilon_{zx} \\ \varepsilon_{xy} \end{bmatrix}$$

Where μ and λ are the Lamé constants for the specific material and are found using the longitudinal and shear sound speeds as discussed later. These constitutive relations simplify further for special states of stress and strain. Through the Lamé constants, additional information may be found that helps to further classify a material. Young's (E), Shear (G), Bulk (K), and Longitudinal (F) moduli are given respectively by:

$$E = \frac{\mu(3\lambda+2\mu)}{\lambda+\mu}$$

$$G = \mu$$

$$\mathrm{K} = \lambda + \frac{2}{3}\mu$$

$$F = \lambda + 2\mu$$

The Poisson ratio of the material gives its "compressibility" and may also be found through the use of the Lamé constants and is given by:

$$\nu = \frac{\lambda}{2(\lambda+\mu)}$$

The Poisson ratio for sand falls between 0.20 and 0.45. The variation in the Poisson ratio for sand is due, in part, to its level of compaction as well as its varying elemental composition.

2. Dynamic Elastic-Plastic Theory

The impact of one material onto another creates two shockwaves, one in each material but travelling in opposite directions. The shockwave in conjunction with the

particle velocity following this shock in the impacted material contains useful information about the elastic and plastic response of the material, and ultimately the failure mechanisms of the material. Information obtained can also be used to infer certain equation-of-state (EOS) properties. In order to acquire this information, it is necessary to have an understanding of what causes these shockwaves to form and the physics behind the processes that occur during the dynamic event. These processes can be characterized by the conservation laws that govern the physical world; conservation of mass, momentum and energy. By examining a shock as it passes through a control volume, one is able to apply the conservation laws at the material interfaces and derive 'jump conditions' that relate the initial pressure, density and energy of the material to the shocked material behind the shock front. The resulting 'jump conditions' are:

$$\frac{\rho_0}{\rho} = 1 - \frac{u_p}{U_S}$$

$$P - P_0 = \rho_0 U_S u_p$$

$$e - e_0 = \frac{1}{2}\left(P + P_0\right)\left(\frac{1}{\rho_0} - \frac{1}{\rho}\right)$$

where,

$\rho_0 \equiv$ Initial density of the material

$\rho \equiv$ Density of the material behind the shock front

$P_0 \equiv$ Initial pressure (stress) state in the material

$P \equiv$ Pressure (stress) state behind the shock front

$e_0 \equiv$ Initial specific energy in the material

$e \equiv$ Specific energy in the material behind the shock front

$u_p \equiv$ Particle velocity behind the shock front

$U_S \equiv$ Shock speed of the shock front propagating through the material

These equations are derived with certain premises about the shock process such as the existence of steady waves. By measuring certain key properties through experimentation and then applying these fundamental 'jump conditions' one is able to

develop an accurate EOS model for the material. The EOS contains fundamental thermodynamic information about the material that can be used to predict the response of the material to arbitrary shock compression. The EOS does not contain any information regarding the elastic-plastic response or dynamic strength of the material. The shock Hugoniot of the material is a representation of the locus of end states of the material properties under dynamic loading. There are several coordinate systems that can be used to represent the Hugoniot of the material of which the shock velocity-particle velocity (U_S-u_p) and pressure-particle velocity (P-u_p) relations are the most common.

When U_s-u_p relations are measured and plotted a linear relationship exists in most cases over a given pressure range. This relationship is represented in equation form as:

$$U_S = C_0 + su_p$$

Research has shown that C_0 is approximately equal to the ambient bulk sound speed of the material. This means that it provides an anchor point for the U_S-u_p relationship as shown in Figure 11.

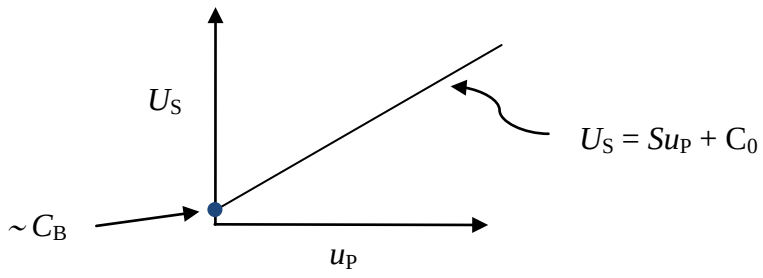

Figure 11. Graphical representation of typical Hugoniot curve in U_S-u_p space

Another common approach used to represent Hugoniot data is to plot the relationship between the pressure and the particle velocity behind the shock front in the material. Pressure is not an easily measured property in dynamic experiments therefore the jump conditions need to be used to *calculate* the pressure. By substituting the above linear relationship between shock and particle velocity into the momentum shock jump condition we obtain the following relationship:

$$P = \rho_0 \left(C_0 + s\left(u_p + u0 \right) \right) \left(u_p - u_0 \right)$$

and it is apparent that pressure has a quadratic dependence on the particle velocity. This provides a functional relationship as shown in Figure 12 for the Hugoniot in P-u_p space. The graphical representation of the Hugoniot in P-u_p space allows for the interpretation of interactions that occur during an experiment with multiple shock interactions which is discussed in more detail later.

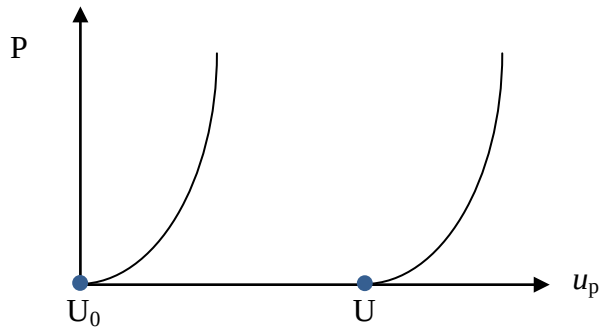

Figure 12. Graphical representation of P-u_p curves for a typical material at different initial values dependent on initial shock condition

Upon characterization of the Hugoniot for a material, an equation of state (EOS) for the material may be developed. The EOS of a material is usually defined by the relationship between pressure, temperature and specific volume (or similar relationships between thermodynamic properties). Shock data may be used to experimentally determine data points to establish the relationship between relevant thermodynamic properties. The P-*v* relationship formed from the jump conditions is given by:

$$P - P_0 = \frac{U_S^2}{v_0} \left(1 - \frac{v}{v_0} \right)$$

and is graphically represented in Figure 13.

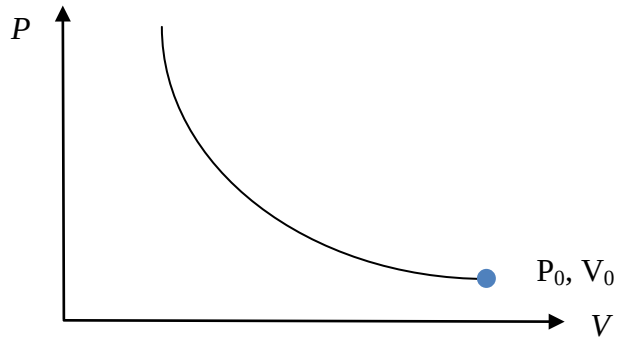

Figure 13. Graphical representation of a typical P-V curve

The curve is a locus of points representing the end states of the shock event and does not represent a continuous path of states through which the material transitions to reach the end state. Instead, the material travels from its initial state to the final state via the Rayleigh line that connects the initial and final state. The slope of the Rayleigh line is given by:

$$slope = -\frac{U_S^2}{v_0}$$

and is depicted in Figure 14.

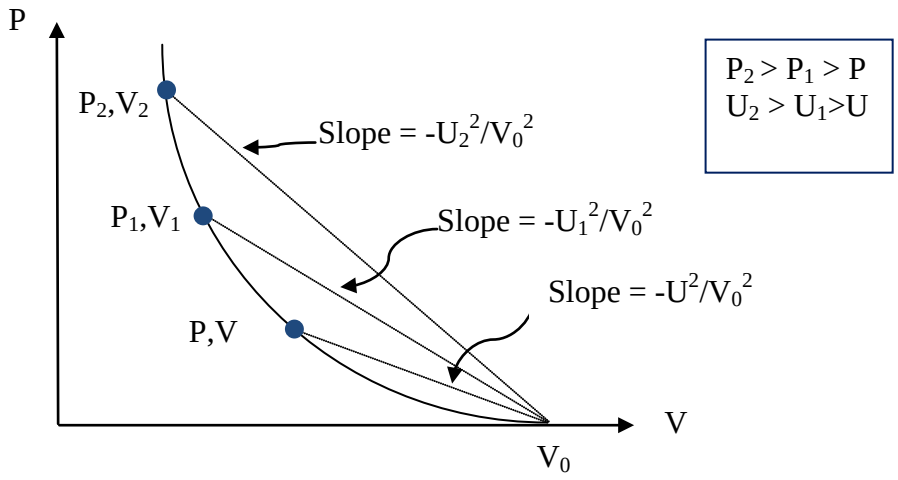

Figure 14. Graphical representation of the initial and final points in P-V space connected by different Rayleigh lines

The Hugoniot in P-V space graphically and analytically represents what occurs during shock compression. The figure shows that the shock speed is dependent upon the end state to which it is being shocked. The higher the pressure to which it is being shocked, the greater the slope of the Rayleigh line becomes, thus increasing the shock velocity. This applies for all simple Hugoniots that have only a single branch. Some Hugoniots have inflection points that result in additional branches and allows the shock response to have more than one stable shock wave.

Given these restrictions combined with the stress tensor for isotropic materials and assuming the direction of interest is in the *x*-direction then the stress strain relationship reduces to:

$$\sigma_x = (\lambda + 2\mu)\varepsilon_x$$

For dynamic yielding experiments the point at which this stress relationship exceeds the dynamic elastic limit is called the Hugoniot Elastic Limit (HEL). Using Young's modulus and rearranging the equation above, the HEL stress is given in terms of Lamé constants and simple yield strength as:

$$\sigma_{HEL} = Y\left(1 + \frac{\lambda}{2\mu}\right)$$

The HEL can also be given in terms of Poisson's ration where Y is the yield point determined from experiments in a condition of uniaxial stress.

$$\sigma_{HEL} = Y\left(\frac{1-\nu}{1-2\nu}\right)$$

This expression allows one to estimate the HEL from measured values of Y.

If the Hugoniot in P-V space has an inflection point then there may be more than one shock as shown in Figure 15. The inflection point will cause a two-wave structure to exist over a given range of pressure. These waves consist of an elastic precursor wave followed by a plastic wave. The elastic wave takes the material to the HEL state and the plastic wave takes it to the final state as shown in Figure 15.

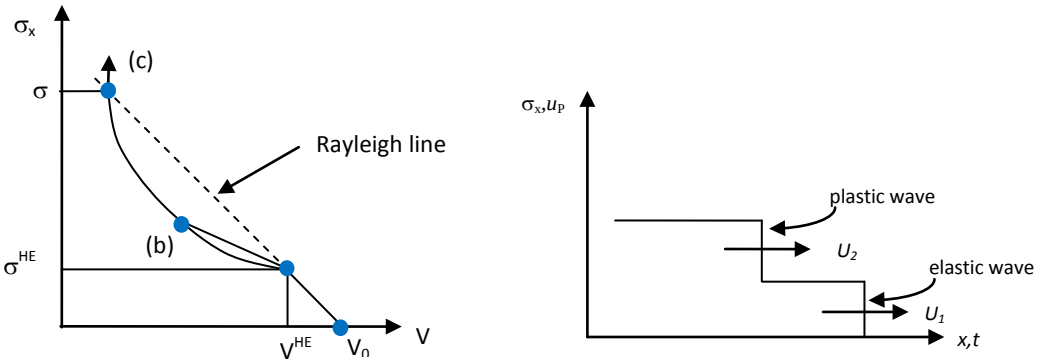

Figure 15. Schematic of plastic and elastic waves travelling through a material in P-V and P-*x* space

The HEL can also be related to the particle speed and volume of the material behind the shock front. The particle velocity of the HEL can be measured through fundamental shock experiments and then, in turn, be used to calculate the dynamic yield point. This relationship is given by:

$$\sigma_{HEL} = \left(\frac{\left(u_p^{HEL} \right)^2}{V_0 - V_{HEL}} \right)$$

Once the materials have been characterized under dynamic loading conditions then the material response can be predicted under other loading conditions.

3. Compression of Granular and Porous Materials

The previous sections focused primarily on the shock theory of solid materials at full initial density. Granular materials and other loose powdered materials have much lower initial densities than actual grains of solid materials due to the voids between the granules. Similarly, pores in solid materials distend them and cause them to have lower initial densities than their crystalline density. This porosity profoundly changes the way that the material responds to dynamic deformation.

a. Dynamic Compression of Porous Materials

In solid materials small stresses and strains are very close to being the same as the shock Hugoniot and the principle isentrope. This allows the Hugoniot to be taken as the release path for a material that has been shock compressed to a certain P-V state as shown in Figure 16.

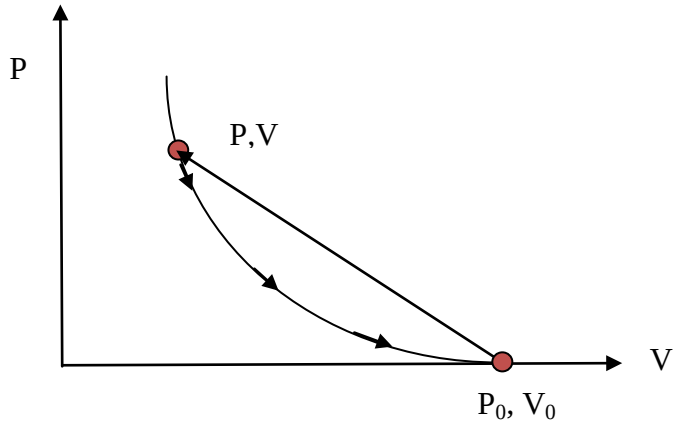

Figure 16. Typical P-V curve for most solid materials

The shock travels along the Rayleigh line from the initial state at P_0, V_0 to the final state at P, V during the compression process. The shock causes a jump from one point on the Hugoniot to another. The release for small stress and strain follows the Hugoniot back down to the initial state and is thus a close approximation to the release isentrope.

For porous materials the loading and unloading paths can be significantly different as shown in Figure 17. The solid Hugoniot is shown as the line from point *c* to point *b*. However, because the material is porous, its initial volume is at point *a*, and thus greater than the full density initial volume *c*. Shock compressing a material with initial volume *a* causes the shock process and states to lie on the diagonal line from *a* to *d* first and then on the full density Hugoniot once the pores are completely "crushed" out. The path from *a* to *d* is called the "crush curve." Once pores are crushed they usually stay crushed so that the release comes back down the Hugoniot from *b* to *c* for low stress.

Since the ambient pressure volume is now a lot smaller than the initial value it is apparent that the compression and release paths are significantly different.

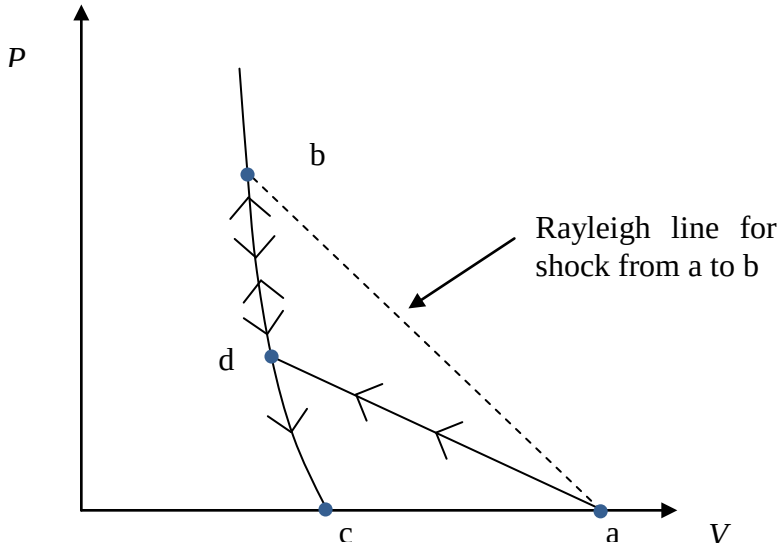

Figure 17. Graphical representation of loading and unloading paths for porous materials

One of the simplest ways developed to model the compression of porous materials is the “snowplow” method. It provides a basic understanding of how porous materials react to compression given the assumptions that there is no resistance to compaction and that the solid P-V Hugoniot is vertical, meaning that the end state for compression is always the same. Figure 18 shows what this looks like in P-V space.

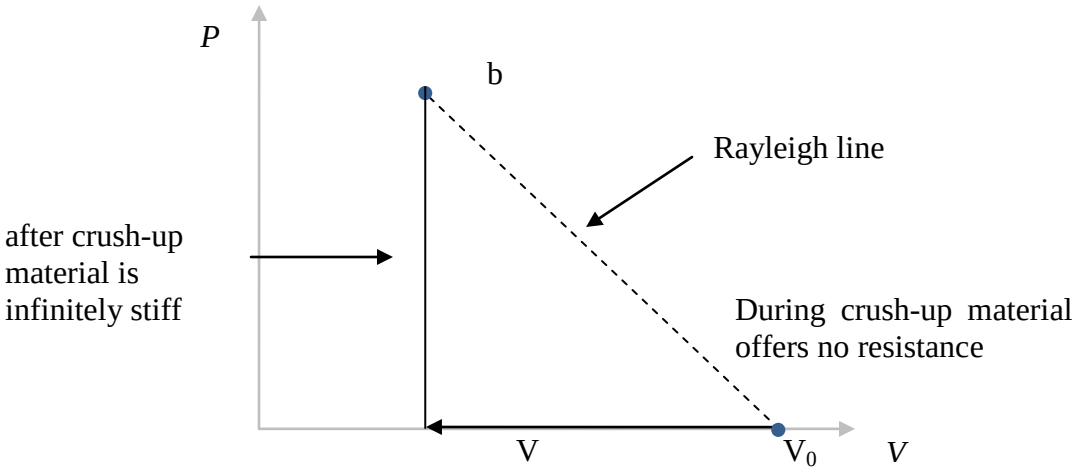

Figure 18. Graphical representation of the “snowplow” model

The “snowplow” model is a limiting case model since after the entirety of free volume is crushed out the Hugoniot is vertical. The degree of porous compaction is defined by the parameter α which is given as:

$$\alpha = \frac{volume\ with\ porosity}{volume\ of\ \ solid} = \frac{V_{00}}{V_0}$$

The parameter α is initially larger than one but approaches one as the pores in the material are crushed out. It has been shown that waves in this type of material are triangular unsteady waves that change as a function of run as shown in Figure 19.

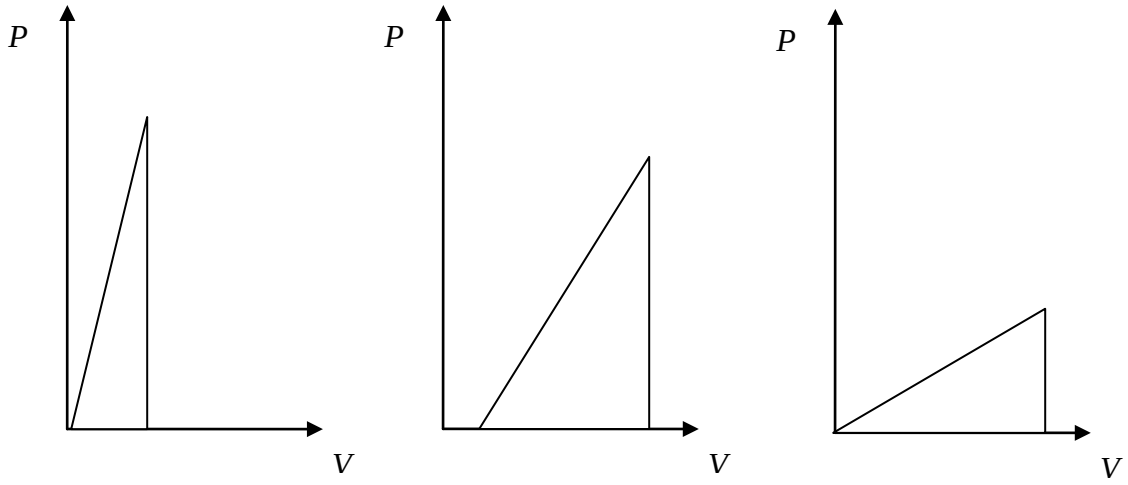

Figure 19. Triangular wave changing as a function of run

The shock and particle velocities for a “snowplow” material are given by:

$$U_S = V_{00}\sqrt{\frac{P}{V_{00}-V_0}} = \sqrt{\frac{\alpha^2 PV_0}{\alpha-1}}$$

$$u_p = \sqrt{P\left(V_{00}-V_0\right)} = \sqrt{PV_0\left(\alpha-1\right)}$$

The momentum of the triangular wave pulses must be conserved which results in the wave attenuating as shown in Figure 20

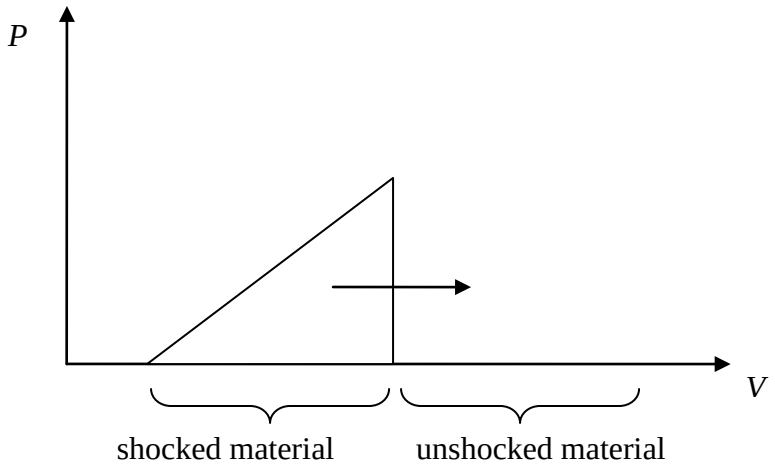

Figure 20. Attenuation of triangular wave due to conservation of momentum

It can be shown that the attenuation of the pressure goes as $1/x^2$ and is given by:

$$P = \frac{I_0^2 V_0 \alpha^2}{(\alpha - 1) x^2}$$

where I_0 is the impulse or the momentum divided by the area. The above equation can be substituted into the shock velocity equation in order to find the attenuation with time. It can be shown that from this the pressure attenuates as $1/t$ and is given by:

$$P = \frac{I_0}{t}$$

Porous materials are good energy attenuators as shown by the energy jump condition:

$$E = \frac{1}{2} P (V_{00} - V)$$

This is shown graphically in Figure 21.

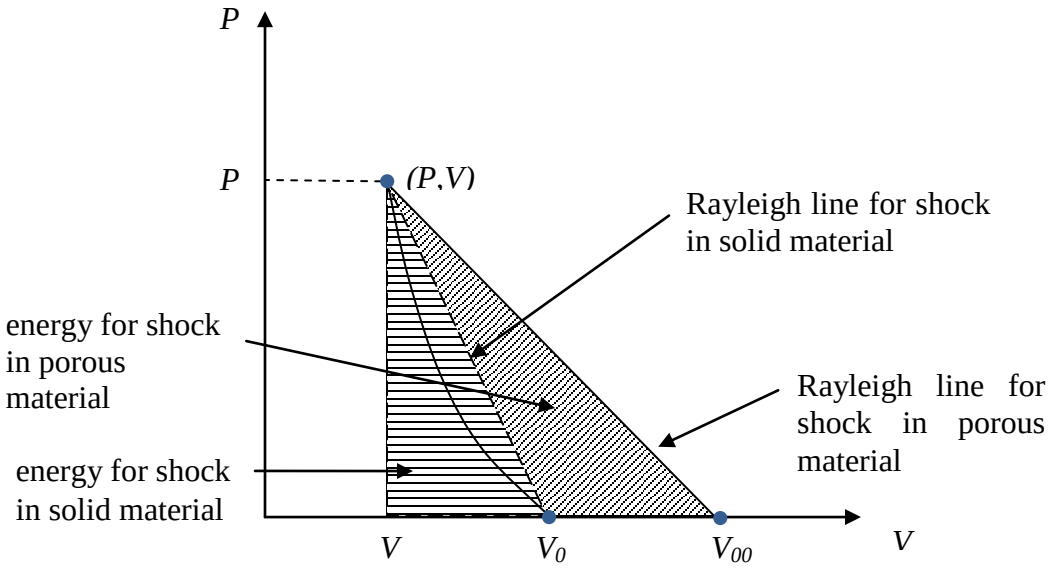

Figure 21. Graphical representation of the energy jump condition for a porous material

The energy behind the shock in a porous material is significantly greater than that for a solid material. There is also significantly more residual energy left behind in the porous material after release in the form of waste heat as shown in Figure 22.

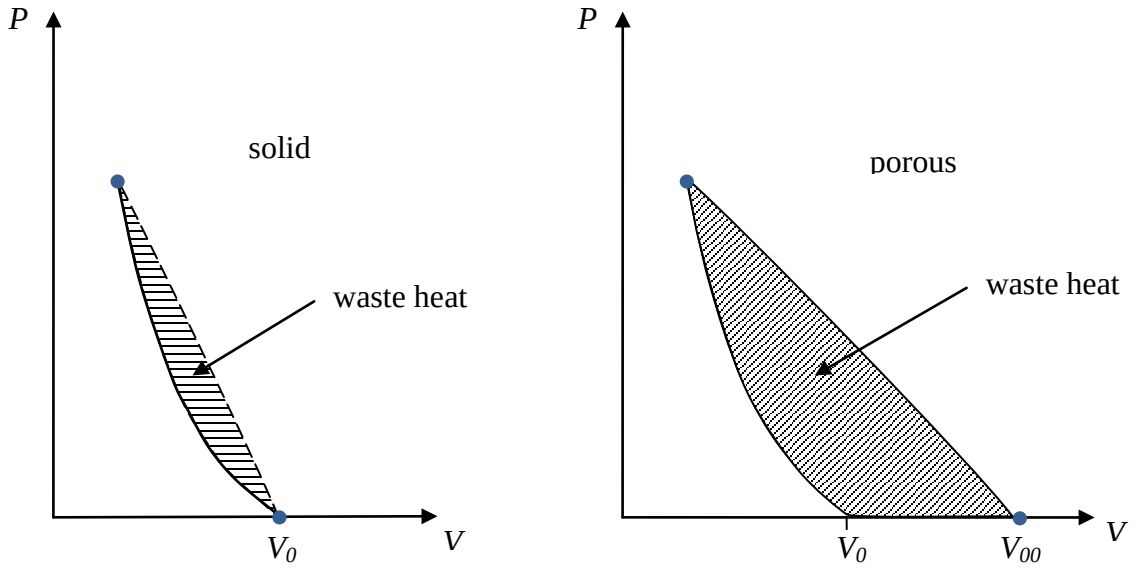

Figure 22. Compare and contrast of waste heat between solid and porous materials

Because this is a good way to convert mechanical energy to waste heat, porous materials are widely used for this application.

For high pressures that result in full compaction of the porous material and where α is above a certain critical value, it is possible to have Hugoniots with positive slopes as shown in Figure 23.

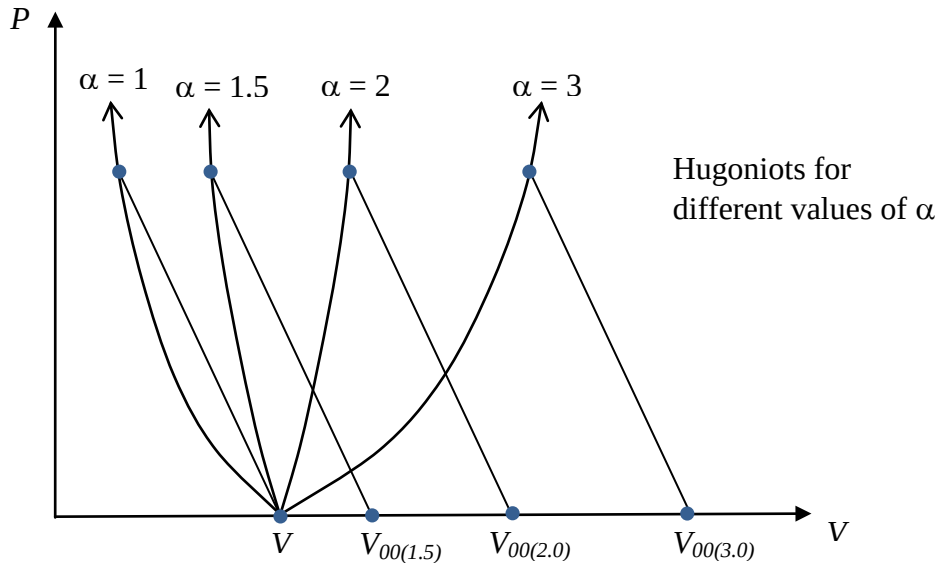

Figure 23. Hugoniots for varying values of α

The positive slopes occur only when sufficient enough heat is generated resulting in a thermal pressure that acts to expand the material.

4. P-α Model

The "snowplow" model provides a good basic understanding of what occurs during the compaction process for porous materials but a better model that is able to represent the true material response is the P-α model developed by Herrmann [4] and it is the model of choice for describing the dynamic response of porous materials. This model is useful at describing the relatively weak shock compaction and partially compacted states. The parameter α is described similarly to before and is given by:

$$\alpha = \frac{\text{volume of distended material}}{\text{volume of solid}} = \frac{V}{V_S}$$

The solid is assumed to obey the equation of state: $P = P\left(V_S, E\right) = P\left(\frac{V}{\alpha}, E\right)$.

Since the new parameter of α has been introduced, a new equation is needed. This equation is taken to be the functional form of α and is given as: $\alpha = \alpha\left(P, E\right)$. This

function represents the amount of irreversible compaction that has occurred at peak pressure P. The value of α is only allowed to decrease and never increase. The behavior of α is graphically represented in Figure 24

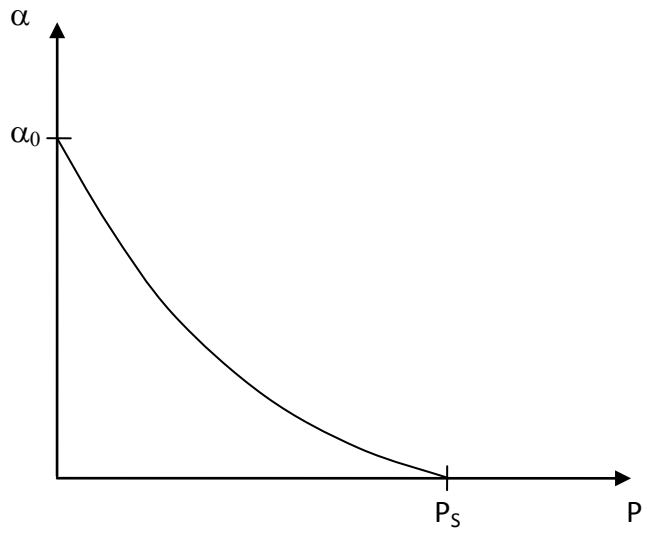

Figure 24. Graphical representation of the behavior of the parameter α

A functional form of the P-α model that is commonly used is:

$$(\alpha - 1) = (\alpha_0 - 1)\left(1 - \frac{P}{P_S}\right)^2$$

This model can be used to describe the partially compacted states and shows that the release paths can be significantly different than the compression paths as shown in Figure 25.

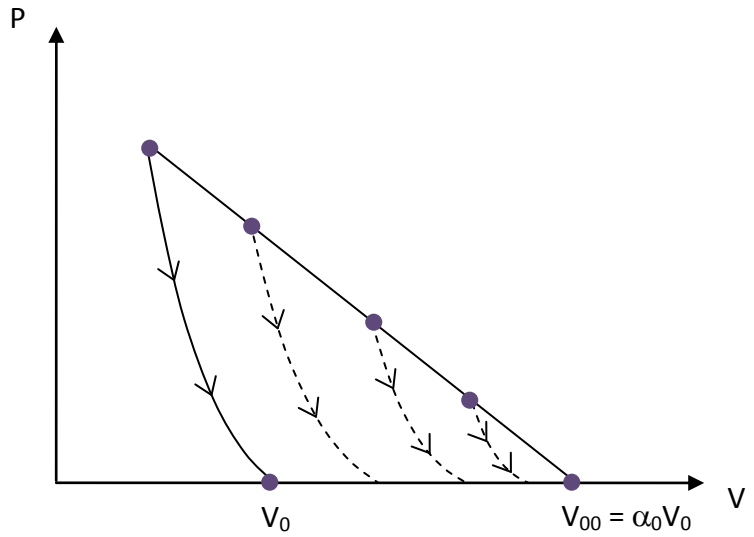

Figure 25. Possible variations in release paths for porous materials

In Figure 25, the material strength was ignored. However, some porous materials will have strength that must be overcome before compaction can occur. For these cases, the P-V curve is graphically represented in Figure 26.

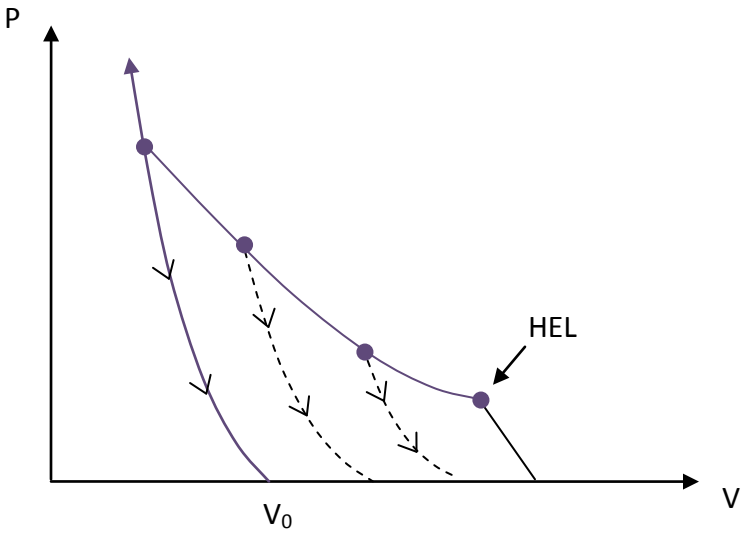

Figure 26. Possible release paths for porous materials with strength that must be overcome prior to compression

This means that for a given range of shock pressures there can be an elastic precursor wave. The release wave speeds in porous materials are always greater than the shock speeds which can cause difficulty during experimentation. The shock is slowed by the collapse of the pores while the release is travelling through a region of increased material density. For unconsolidated porous materials the mechanical strength may be quite small and will result in a very small or no elastic wave.

B. SAMPLE CHARACTERIZATION

In order to accurately predict the response of materials using the shock theory reviewed above, some measurements of the initial properties of the sample materials must be made. The most useful measurements that can be made are the initial density of the material and the shear and longitudinal sound speeds.

1. Initial Density

Initial sample density is measured by determining the sample mass and volume and then using the basic formula: $\rho_0 = \frac{m}{V_0}$. Mass can usually be measured easily and on an accurate scale with standard laboratory equipment. Volume can be determined for regular objects by using dimensions and then volume formulae. Due to the granular nature of sand this method was used vice more accurate immersion techniques based on Archimedes principle. The initial volume of the technical sand was determined by filling a cylinder and cap of known measurements and then inserting the cap and measuring the displacement of the cap from the top of the cylinder. The initial density of the technical sand was determined in its non-compacted natural state by taking the average of multiple density measurements given varying masses and volumes for each specific test sample. The literature values for density will be used for the more common materials used in the experiments as these values are well established and highly accurate.

2. Elastic Sound Speeds

In order to determine the elastic constants of the isotropic materials used in this research, the elastic sound speeds of those materials were measured. The method used to calculate the sound speed of these materials is based on the relationship of velocity proportional to time of travel and distance given by:

$$c = \frac{x_{sample}}{t_{transit}}$$

The method used to obtain the sound speeds requires the thickness of the sample to be measured and to then send an ultrasonic pulse through it using an ultrasonic transducer and then use a high precision digitizer to measure the transit time through the material. The transit time is indicated by the pulse echoes detected by the digitizer as shown in Figure 27.

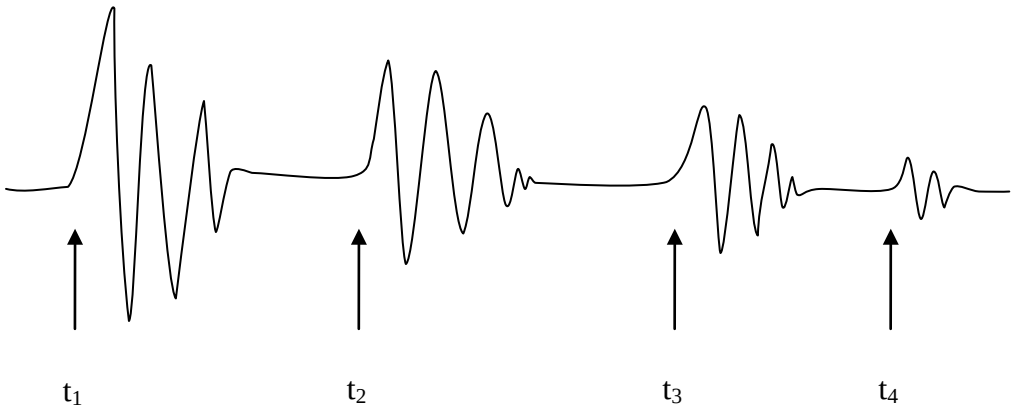

Figure 27. Schematic representation of pulse traces from sound speed measurements

The time between each pulse is the time it takes the pulse to complete a round trip though the sample as shown in Figure 28. The time used for calculations is therefore half of this round trip time.

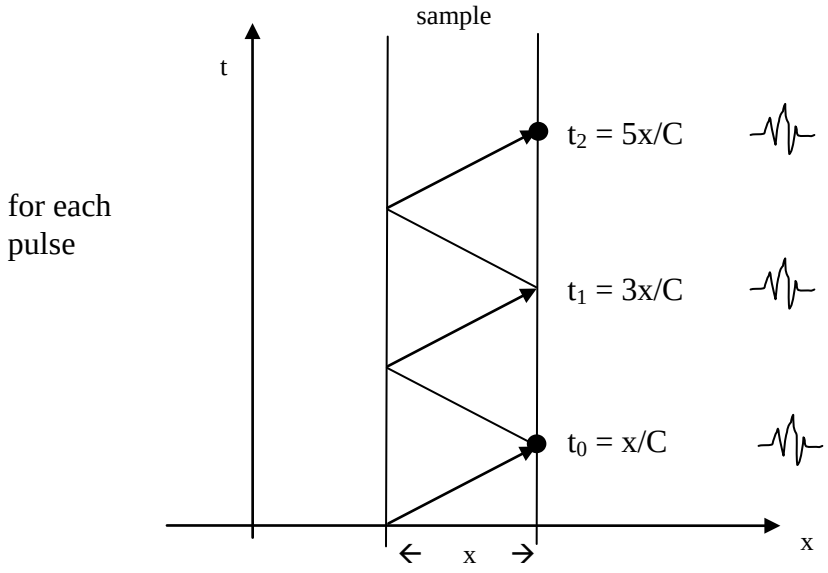

Figure 28. Schematic relating time measurements to pulse waves in sound speed measurements

A linear regression analysis is applied to the times to obtain a least squares fit to the data. The slope of the best fit line coincides with the sound speed of the material as shown in Figure 29.

x	t
$2x_1$	t_1
$4x_2$	t_2
$6x_3$	t_3

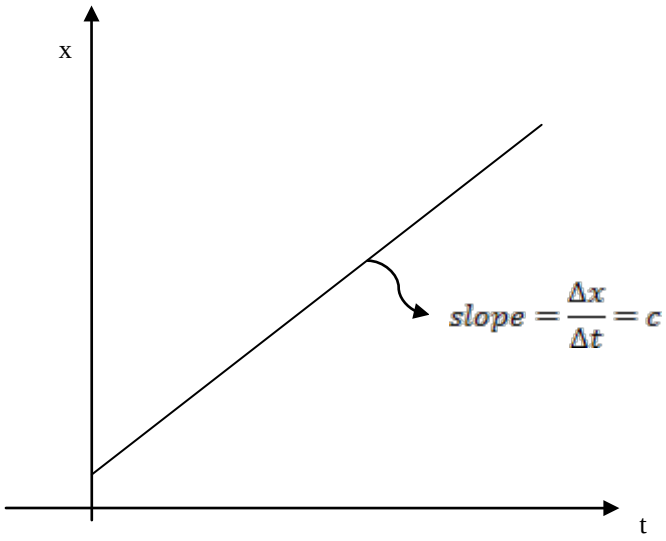

Figure 29. Schematic representation of linear regression analysis to obtain sound speeds

Once the sound speeds have been measured, they may then be used to find the elastic constants of isotropic materials. These constants are easily calculated through the use of the relationships between longitudinal (C_L) and shear (C_S) sound speeds and the elastic constants of isotropic materials.

$$C_L = \sqrt{\frac{\mu}{\rho_0}}$$

$$C_S = \sqrt{\frac{\lambda + 2\mu}{\rho_0}}$$

Given the longitudinal and shear velocities, the two Lamé constants λ and μ can be determined.

The bulk sound speed for the material may now be calculated since the longitudinal and shear sound speeds are known as shown by:

$$C_B = \sqrt{C_L^2 - \frac{4}{3}C_S^2}$$

This is a useful quantity in shock wave experiments. However, due to the porous nature of the technical sand this method for determining the longitudinal and shear sound speeds does not work. This method is still useful in determining these values for the isotropic materials used in the experimental process.

An ultrasonic pulse-echo transducer receiver system manufactured by Olympus was used in conjunction with a digital oscilloscope to measure the elastic sound speeds of the isotropic materials used during the course of this research. Figure 30 shows the physical set up used to take the sound speed measurements.

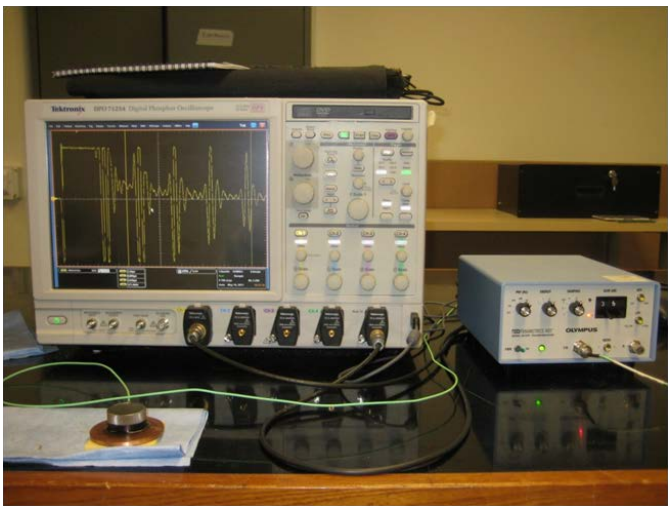

Figure 30. Oscilloscope and ultrasonic pulse-echo transducer

Table 1 provides a summary of these measurements as well as the established literature values for them.

Table 1. Summary of measured sound speeds compared to literature values

	Measured for this Research		Literature Values	
Material	C_L(mm/μs)	C_S(mm/μs)	C_L(mm/μs)	C_S(mm/μs)
Aluminum T-6061	6.31	3.10	6.40 [4]	3.15 [5]
Copper OHFC (Annealed)	4.80	2.26	4.76 [4]*	2.33 [5]*
Copper OHFC	4.70	2.30	4.76 [4]	2.33 [5]
Sand				
Technical Sand				

*There is no distinction in the literature values between annealed and non-annealed OHFC copper.

Due to the granular nature of sand which causes it to be highly dispersive, a valid sound speed was unable to be obtained with the equipment available and literature values were likewise unable to be found.

C. HUGONIOT MEASUREMENT EXPERIMENTS

1. Shock Compression Experimental Techniques

A shock moving through a material can be characterized by the shock jump conditions:

$$\frac{\rho_0}{\rho} = 1 - \frac{u_p}{U_S}$$
$$P - P_0 = \rho_0 U_S u_p$$
$$e - e_0 = \frac{1}{2}(P + P_0)\left(\frac{1}{\rho_0} - \frac{1}{\rho}\right)$$

These three equations contain five unknowns meaning that they cannot be resolved analytically without additional information. The shock velocity and the particle velocity are the two values that are usually found experimentally in order to solve these equations. The measurement of the shock and particle velocities over a range of pressures can then be used to formulate the Hugoniot EOS for the material.

A large part of this research focused on the establishment of the methodology and the creation of the processes to be followed in order to allow successful shock compression experiments on granular and porous media at the NPS impact laboratory. The following sections cover the initial design concept and its evolution. Additionally, during this process a build sheet was created to ensure all pertinent pre-shot data will be recorded during the buildup of an experiment. This build sheet is presented in Appendix A.

a. Target

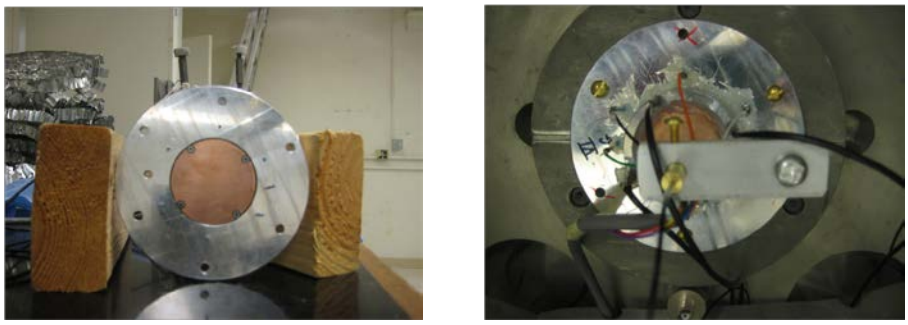

Figure 31. Front and rear view of target assembly

In order to perform a gas gun experiment, a target assembly and a projectile are needed. The target assembly that was used for the technical sand experiments is shown in Figure 31. The target design was based on the target design used for experimentation with cerium oxide (CeO) powder, a low initial density powder, conducted by [6]. The target consists of the basic subcomponents of: target plate, barrel assembly, VISAR probe, velocity pins, piezoelectric pins, and the material sample.

(1) Target plate. The first component used to build the target is the target plate. Figure 32 shows the target plate design used for this research. The target plate is the foundation of the target to which the other components must attach. The target plate was fabricated from 6061 Aluminum and was modified as required for each individual experiment.

Figure 32. Target Plate

(2) Barrel assembly. Due to the granular nature of the technical sand, a containment apparatus was needed to constrain the technical sand during the experimental process. The barrel assembly was fabricated from 6061 Aluminum and had a copper base plate that allowed for a symmetric impact with the copper impactor. Aluminum and copper were selected based on the barrel assembly design used for the CeO powder. The barrel had four holes bored through the side walls to allow for the insertion of the piezoelectric pins into the apparatus. The completed barrel assembly is shown in Figure 33.

Figure 33. Barrel assembly

(3) Velocity Inteferometer for Any Reflector (VISAR). The diagnostic tool VISAR can be used to measure the particle velocity at the rear surface of most materials being studied. However, for granular and porous materials like the technical sand this is not always possible. Still, VISAR is used to record the time that the shock wave arrives at the rear surface of the material being tested. VISAR is a velocity interferometer that has been widely used and developed for use in shock compression experiments. A general experimental setup used for VISAR is shown in Figure 34. The VISAR for this research was manufactured and procured from National Security Technologies (NSTEC). Hemsing [7] et al. provides detailed analysis and operation of the VISAR system.

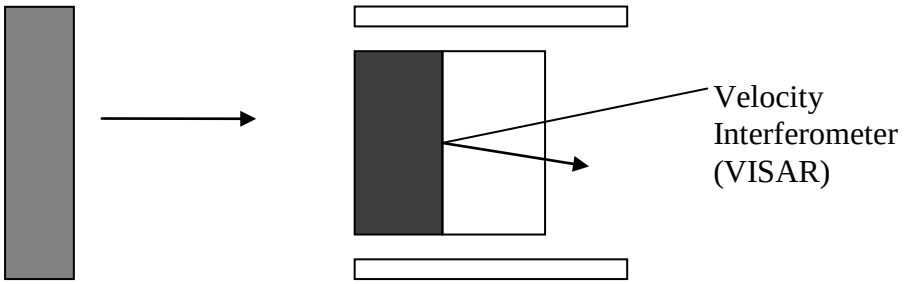

Figure 34. Representation of VISAR system used in shock compression experiments

(4) Velocity pins. For this research velocity pins were used to obtain an accurate measurement of the velocity at which the projectile impacts the target assembly. The velocity pins are electrically conductive metallic pins that short a charged capacitor in an RC circuit, causing a fast rising pulse to be generated that is recorded on a digitizer. Six pins are arranged in a circular pattern around the material sample at an equidistant radius from the center of the target plate and are at 60 degree intervals. Additionally, the velocity pins are stepped down with each pin protruding from the surface of the target plate at a fixed decreasing interval. The measured pulse times are then used to perform a least squares fit in order to determine the arrival times which are then used to calculate the projectile velocity at impact.

$$v_{projectile} = \frac{\Delta x_{pins}}{\Delta t_{pulse}}$$

The velocity of the projectile is then used during the numerical analysis of the experiment. The regression fit is also used to determine the tilt of the projectile at the point of impact.

(5) Piezoelectric Pins. Impact triggered piezoelectric (PZT) pins are used to trigger the data collection process and to record the initiation of the shock propagation through the sample. These PZT pins are small diameter, commercially procured lead-zirconium-titinate pins. A single PZT pin is set flush with the face of the target plate and is used as the trigger mechanism for the high speed oscilloscopes used to record the data from the diagnostics. Two PZT pins are diametrically opposed and

mounted in the barrel assembly so that they are as flush as possible with the copper base plate in order to obtain time fiducials that are used to obtain the shock initiation time within the sample. These times will have slight variation due to projectile tilt and flushness which is taken into account when determining the shock initiation time from the pin signals.

(6) Window. A polymethyl methacrylate (PMMA) window is used to cap the sample within the barrel assembly and allows for the VISAR to collect data from the rear of the sample. The PMMA window is machined to fit snugly inside the barrel and epoxy is used to secure it so that the sample is contained with no freedom of movement allowed.

(7) Sample. The final aspect of the target assembly is the sample itself. For this research the sample material was spherical glass beads or technical sand. The sample was poured into the barrel assembly to the approximate desired thicknesses. Once poured into the barrel assembly the PMMA window was inserted until flush with the sample and no freedom of movement was detectable. The final thickness of the sample was determined by the measuring the distance from the bottom of the copper base plate to the top of the PMMA window and subtracting the known height of the window and foil. Once the sample is properly prepared it is inserted into the center of the target plate and secured with epoxy.

b. Projectile

Figure 35. Low speed aluminum projectile with copper impactor on left and high speed magnesium projectile with copper impactor on right

Figure 35 shows two different projectiles that were used for this research. The components used in building the projectile are the casing and the impactor. Required measurements were recorded in accordance with Appendix A.

(1) Impactor. The first component of the projectile is the impactor. The impactor is a right circular cylinder with dimensions to match the requirements of the experiment. It is also fabricated from the material of choice based on the requirements of the experiment. For symmetric impact experiments, the target sample or cover plate and impactor are of the same material. The impactor is then lapped to within +/- 10μm of flatness and inserted into the bullet.

(2) Casing. The second component of the projectile is the casing. The casing is the carrier for the impactor and is what is accelerated to the required experimental velocities. The casings used for this research were fabricated from either aluminum 6061 or magnesium. After fabrication the face of the casing is lapped to within +/- 10 μm of flatness. The face of the casing then has a cavity bored out that is of

the same dimensions of the impactor. There is a step placed within the cavity for the impactor to rest and to allow for bonding material to be placed between the casing face and the bottom of the impactor in order to hold the impactor in place during experimentation. This step also allows for a free surface behind the impactor. A small semi-circle section is also drilled out on the edge of the cavity in order to allow any air between the impactor and the casing face to escape when the system is being pumped down to near vacuum.

c. NPS Gas Gun Facility

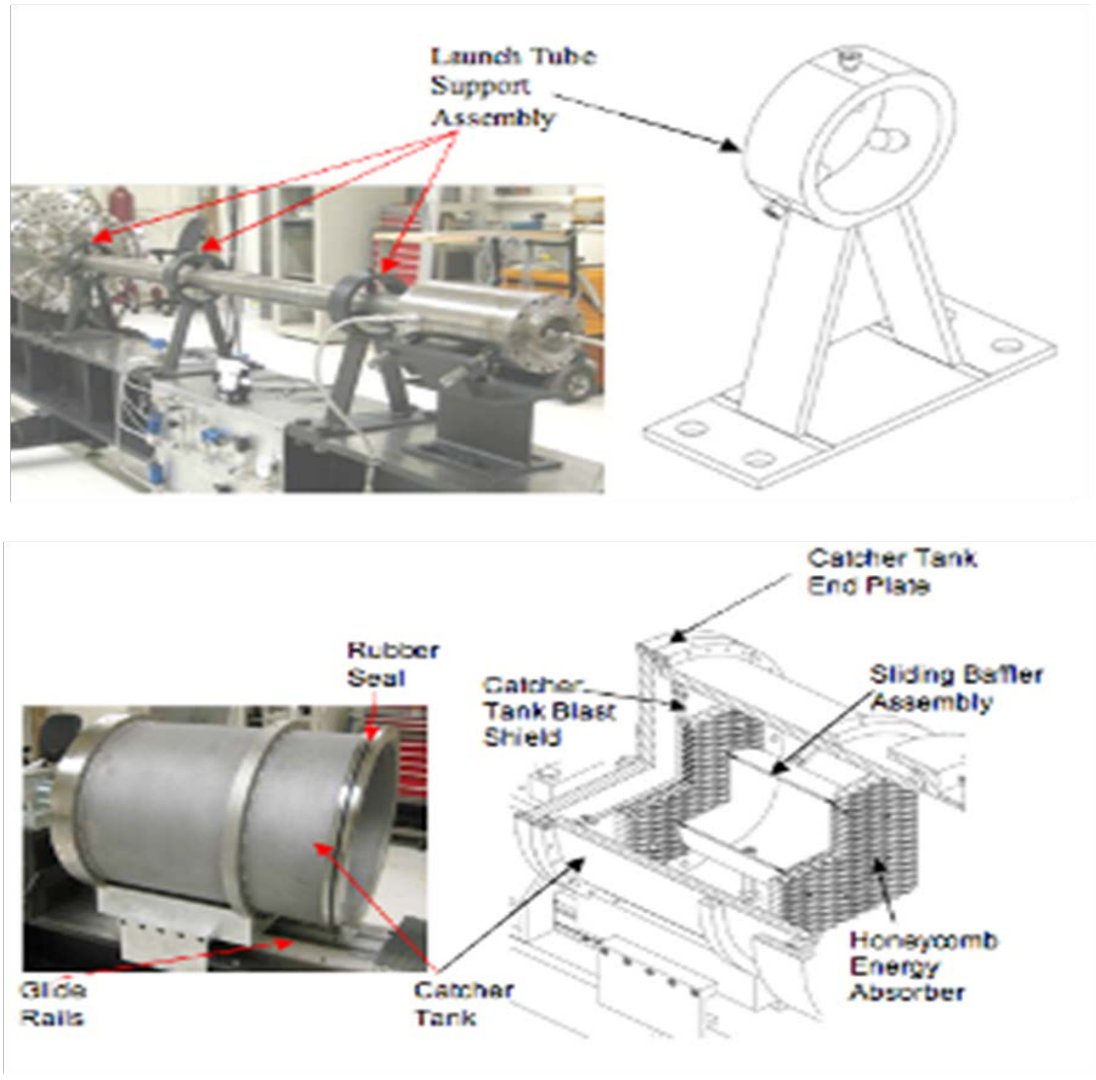

Figure 36. Naval Postgraduate School low pressure gas gun at the Impact Physics Laboratory

The final piece of equipment needed to perform shock compression experiments is the launcher responsible for accelerating the projectile to impact velocity. For this research a single stage light gas gun located at the Impact Physics Laboratory at the Naval Postgraduate School was used. The assembly, testing and operation are outline by Ho [8] and improvements were performed by Denzel [9]. The standard operating procedure was developed by Garner [10] with minor modifications made to it for the purposes of this research and is contained in Appendix B.

2. Hugoniot Measurements

The fundamental of shock physics used to develop accurate EOS models for materials are found in the shock jump conditions:

$$\frac{\rho_0}{\rho} = 1 - \frac{u_p}{U_S}$$
$$P - P_0 = \rho_0 U_S u_p$$
$$e - e_0 = \frac{1}{2}(P + P_0)\left(\frac{1}{\rho_0} - \frac{1}{\rho}\right)$$

The shock speed and particle velocity behind the shock front are the parameters that need to be measured through experimentation at various driver velocities in order to resolve the shock jump conditions. The first parameter measured is the shock velocity which is calculated using the transit time that the shock takes to travel through the sample as shown in Figure 37.

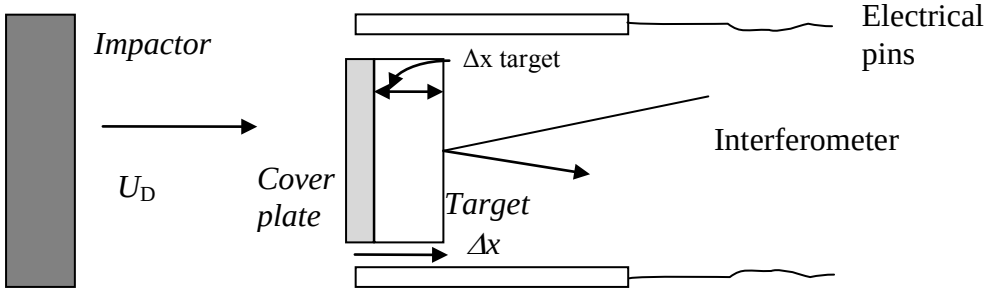

Figure 37. Representation of shock experiment

The shock transit times are calculated using timing fiducials obtained from PZT pins that are flush with the cover plate and sample and the shock arrival times at the back of the sample from the time-resolved back surface velocity profile measured with the VISAR diagnostic system. There is some hysteresis that occurs from the VISAR system and PZT pins which is compensated for by measuring the delays and then applying the appropriate correction factor. Once the transit time is calculated, a simple velocity relationship is used to determine the shock velocity through the sample.

The particle velocity for symmetric impacts can be shown to be half of the flyer or impactor velocity. This is shown graphically in Figure 38 by superimposing a Hugoniot for the flyer and target on the same plot. The two Hugoniots intersect at a common state between the flyer and target given by the jump conditions.

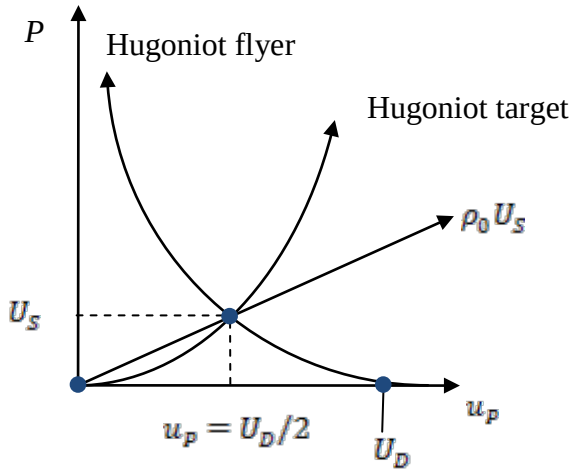

Figure 38. Graphical representation of interactions between flyer and target for a symmetric impact

This same approach may be used for non-symmetric impacts provided that the Hugoniot for the impactor material is known. Determining the particle velocity through experimentation is more difficult. Usually, when performing an experiment to determine the target sample particle velocity, a window is used on the back of the sample in order to prevent a free surface release at the back of the sample. The particle velocity measured by the VISAR diagnostic is not the particle velocity behind the shock front in the sample but rather the particle velocity at the interface of the two materials as shown in Figure 39.

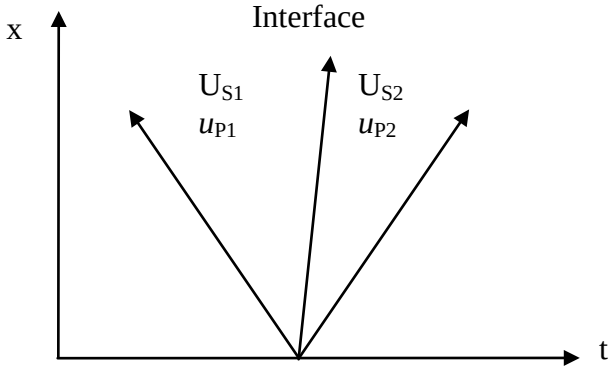

Figure 39. Graphical representation of two materials in contact during a shock event

The wave interactions at the rear surface of the sample and the front of the window occur according to the shock impedance of each of the materials. The particle velocity calculated through the impedance matching method is the particle velocity in the target material in relation to the measured interface particle velocity from the VISAR data. This is a key point, as this relation allows the calculation of the particle velocity that is behind the incident shock in the target sample from the measured interface velocity. It is the particle velocity behind the incident shock in the target sample that is needed to determine a Hugoniot point for the target sample.

This shock impedance matching technique must also be used to determine the particle velocity of the technical sand when calculating it in the forward direction, which is preferred, and is described below for the interaction between the cover plate and target sample. Shock impedance is defined as:

$$Z_{shock} = U_S \rho_0$$

For an initially right going wave in the cover plate, labeled material A, and the target sample labeled material B, the interactions at the surface between these materials follow the impedance matching rules: (1) if $Z_A > Z_B$ a release wave will be reflected back into the material A and the resulting pressure in both A and B will be less than the initial pressure in material A and (2) if $Z_A < Z_B$ a re-shock will occur with the resulting pressure in both A and B will be greater than the initial pressure in A. This is shown graphically in Figure 40 for the case of $Z_A > Z_B$.

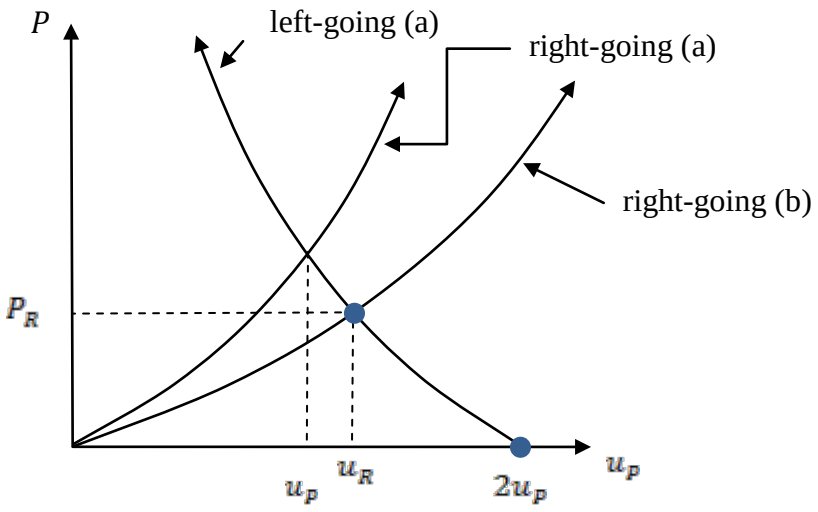

Figure 40. Representation of wave interactions used for impedance matching technique in P-u_p space

The initial and final states in the target material are then linearly connected by:

$$P_A - P_B = -Z_A(u_A - u_B)$$

Using the relation from the jump conditions:

$$P = Z\boldsymbol{u}_p$$

The final particle velocity in the target sample can be found to be:

$$u_B = u_A\left(\frac{\rho_{0_A}}{\rho_{0_B}}\right)\left(\frac{U_{S_A}}{U_{S_B}}\right)\left(\frac{2Z_B}{Z_B + Z_A}\right)$$

Now that the shock velocity, particle velocity and pressure are all known, there is enough information to determine a point on the Hugoniot for material A.

3. Edge Releases

When performing shock compression experiments, edge releases from the target sample must be accounted for. Edge releases occur when the shock front interacts with the edge interface of the target sample and causes a release that travels sideways into the target sample. This release interacts with the shock front as it travels through the target sample normal to the impact plane. For isotropic materials, the time at which the edge

release reaches the back of the target sample may be estimated given the assumption that the release wave travels at a forty five degree angle from the edge of the sample. This estimation requires the longitudinal sound speeds of the impactor and target material, measured according to the techniques discussed earlier. For the technical sand an estimate must be made for the longitudinal sound speed as a longitudinal sound speed measurement cannot be made with the equipment available. Letting *l* be the thickness, or length that the lateral shock must travel through, of the target material, and *r* be the radius of the target sample, the time that the edge release reaches the rear surface of the target material for cases in which $C_i > C_t$ can be approximated by:

$$t \approx \frac{r}{C_i} + \frac{l}{C_i}\sqrt{\frac{C_i^2}{C_t^2} - 1}$$

Where C_i and C_t are the ambient longitudinal sound speeds of the impactor and target respectively. This approximation allows the experimentalist to ensure that the target is thin enough and has a large enough radius such that the edge release wave does not overtake the shockwave prior to it reaching the rear surface of the target material.

4. Uncertainty Analysis

To completely understand the dynamic events that occur during a shock compression experiment, an understanding of the error involved in the measurements being taken during the experiment and the values that are calculated from those measurements is needed. For a general equation of K:

$$K = F\left(A, B\right)$$

the uncertainty of Z is dependent on the uncertainty of the parameters A and B and given by:

$$\Delta \mathrm{K} = \left(\left(\frac{\partial F}{\partial A} \right)^2 \Delta \mathrm{A}^2 + \left(\frac{\partial F}{\partial B} \right)^2 \Delta \mathrm{B}^2 \right)^{1/2}$$

This general expression for uncertainty may then be applied to the specific parameters measured and calculated in this research. Parameters focused on during this research are the ambient density of the technical sand, shock velocity, stress state, shock impedance, and the associated particle velocities achieved for each experiment.

The ambient density of the technical sand in this research is dependent upon the volume measurements and the mass measurements of the sand used in the target sample. Therefore, the error in the calculated ambient density can be shown to be:

$$\Delta\rho_0 = \left(\left(m\Delta V \right)^2 + \left(V\Delta m \right)^2 \right)^{1/2}$$

The shock speed in this research is dependent upon the factors of distance and time. The error in calculated shock speed can be shown to be:

$$\Delta U_S = \left(\left(\frac{\Delta x}{t} \right)^2 + \left(\frac{x\Delta t}{t^2} \right)^2 \right)^{1/2}$$

and the fractional uncertainty in the calculated shock speed is:

$$\frac{\Delta U_S}{U_S} = \left(\left(\frac{\Delta x}{x} \right)^2 + \left(\frac{\Delta t}{t} \right)^2 \right)^{1/2}$$

The stress state achieved during the shock event depends on the initial density, shock speed and particle speed. The error in the stress can be shown to be:

$$\Delta P = \left(\left(U_S u_p \Delta\rho_o \right)^2 + \left(U_S \rho_o \Delta u_p \right)^2 + \left(\rho_o u_p \Delta U_S \right)^2 \right)^{1/2}$$

The fractional uncertainty is then given as:

$$\frac{\Delta P}{P} = \left(\left(\frac{\Delta\rho_o}{\rho_o} \right)^2 + \left(\frac{\Delta U_S}{U_S} \right)^2 + \left(\frac{\Delta u_p}{u_p} \right)^2 \right)^{1/2}$$

The shock impedance error can be similarly determined and can be shown to be:

$$\Delta Z = \left(\left(U_S \Delta\rho_o \right)^2 + \left(\rho_o \Delta U_S \right)^2 \right)^{1/2}$$

Determining the formal uncertainty in the particle velocity is significantly more complicated in this case as the interface has to be accounted for. Instead of determining the formal uncertainty for the particle velocity, due to not knowing the VISAR free surface particle velocity, which is needed, a standard approach was taken to determine the uncertainty of the particle velocity instead. The upper and lower bounds of the particle velocity were determined based on the upper and lower error bounds found for the shock velocity and initial density. By calculating the upper and lower bounds of the particle velocity in this way, adequate experimental error is able to be determined. These equations and analysis will be used to compute the uncertainty of the measured and calculated parameters of interest for this research.

THIS PAGE INTENTIONALLY LEFT BLANK

III. EXPERIMENTAL SETUP AND RESULTS

A. TECHNICAL SAND HUGONIOT SHOTS

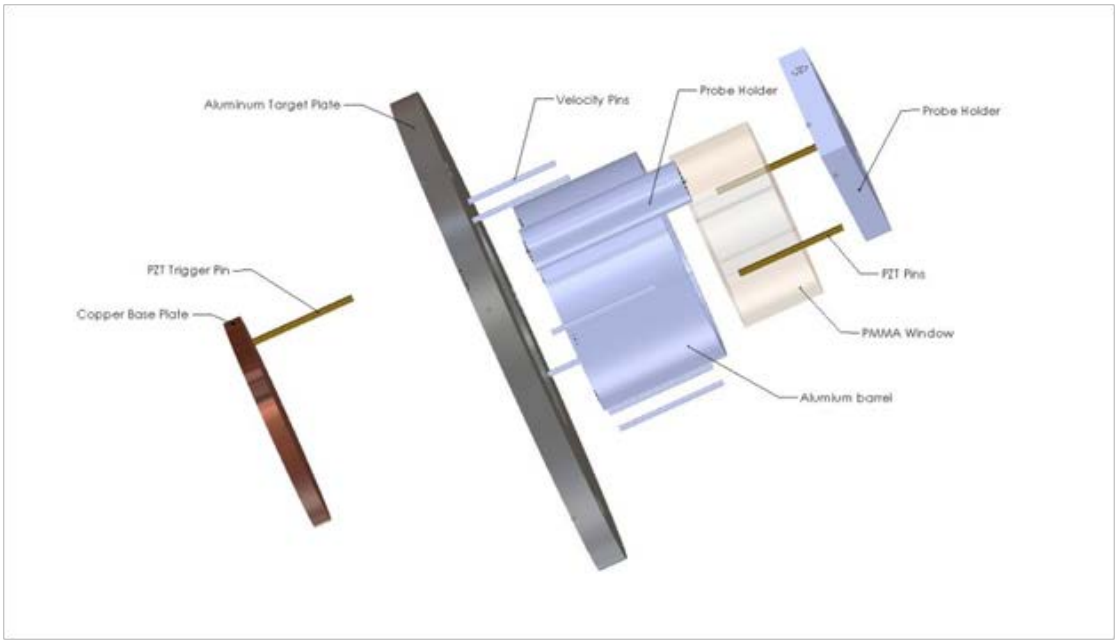

Figure 41. Schematic representation of target assembly

Figure 41 shows a schematic representation of the main elements of the target setup for the experiments performed in this research. As can be seen, the sample consists of a barrel and cover plate that holds the technical sand. It is then backed by a viewing window of PMMA that completes the containment apparatus for the technical sand. Diagnostics used in these experiments were single point VISAR, two diametrically opposed PZT pins for measuring a reference time at the front of the target sample and six velocity pins at a fixed radius at sixty-degree intervals around the target sample and stepped protrusion lengths for projectile tilt and velocity measurement. The initial thickness of the copper impactor was eight millimeters and the copper cover plate was four millimeters. These thicknesses were reduced in later shots to thicknesses of four millimeters for the copper impactor and two millimeters for the copper cover plate. This

will allow higher projectile velocities to be reached in follow-on research. A total of three successful shots of this nature were completed at the Impact Physics Laboratory at NPS and are discussed below.

1. NPS Shot 11_03

Shot 11_03 was the third and final proof of concept shot for the target and bullet design. Its success allowed for data collection and analysis. As mentioned above, the copper impactor was eight millimeters in thickness and the copper cover plate was four millimeters in thickness. In order to anticipate the results of the experiment, a rough hand calculation was performed using assumptions to predict the expected results. A copper to copper symmetric impact was used allowing for simpler calculations at the interface between the copper base plate and the technical sand. Using known Hugoniot data as found in Marsh [5] and data from Brown [3] et al., a desired projectile velocity of 0.264 mm/μs, and approximating the velocity of the longitudinal sound speed through the technical sand at pressure to be 10% faster than the shock speed yields a sound speed 0.88mm/μs, an approximate x-t diagram was constructed to represent the anticipated results as shown in Figure 42.

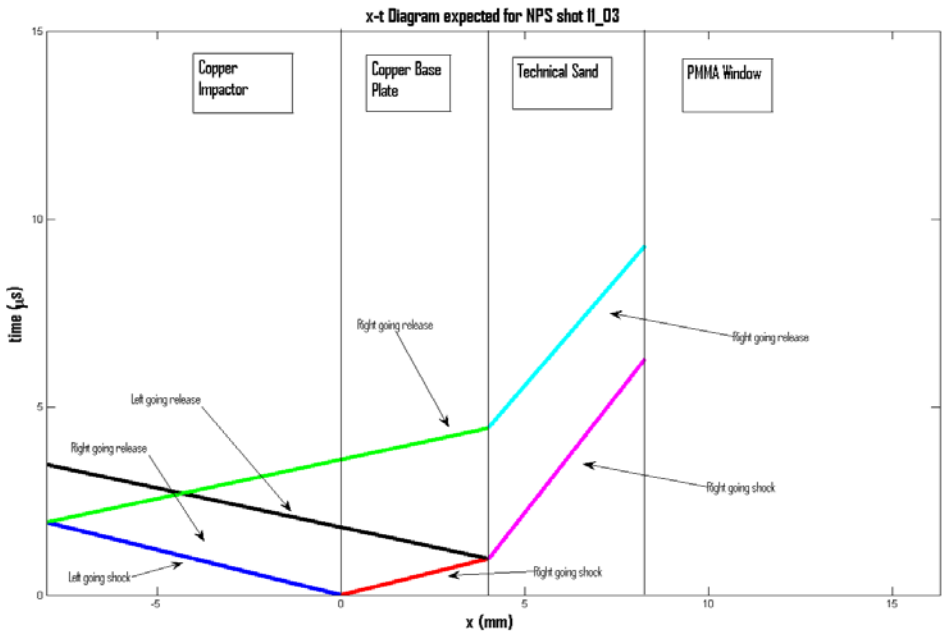

Figure 42. Preliminary x-t diagram for NPS shot 11_03

The anticipated arrival time of the shock wave at the target-window interface was 6.304μs after impact and the expected arrival of the release at the target-window interface was 8.706 μs later. Using the measured diameter for the target sample, the releases were expected to pinch off through the wave at 8.602μs after impact. Also of concern is the shock traveling through the aluminum barrel and then sideways through the PMMA window to the diagnostics. However, as long as the target sample does not exceed a certain critical thickness calculated for each shot, then this additional edge effect will not affect data collection. For this shot, the shock arriving from the side arrived 3.68 μs after the event of interest occurred.

To achieve the desired projectile velocity of 0.264 mm/μs, using a projectile mass of 603.6 grams, the breech pressure that was required was 850 psi. The final dimensions of the copper impactor were 60.03 mm in diameter and 8.017 mm in thickness. For the copper base plate they were 50.02 mm in diameter and 3.996 mm in thickness. The final dimensions of the technical sand were 41.97 mm in diameter and 4.27 mm in thickness.

The shot was successful. All flush pins and velocity pins triggered as expected providing good signal for projectile velocity, projectile tilt and a time fiducial marking the time of shock arrival at the copper base plate and technical sand interface. Usable VISAR data was obtained from the diagnostics that allowed for calculation of shock arrival time at the technical sand and PMMA window interface. However, the intensity of the VISAR rapidly dropped off after impact not allowing for sufficient data collection to determine what occurred after the arrival of the shock at the interface. The VISAR intensity record is shown in Figure 43.

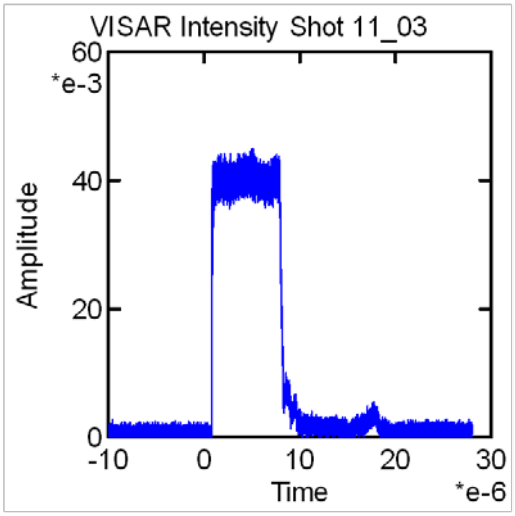

Figure 43. VISAR Intensity for NPS Shot 11_03

Once the VISAR intensity drops off, the data collected afterwards cannot be reliably used. Therefore, during analysis of the shot, a lost fringe must be accounted for at the time of the loss of intensity. Taking the lost fringe to occur at 7.886 μs the analyzed VISAR record is as shown in Figure 44.

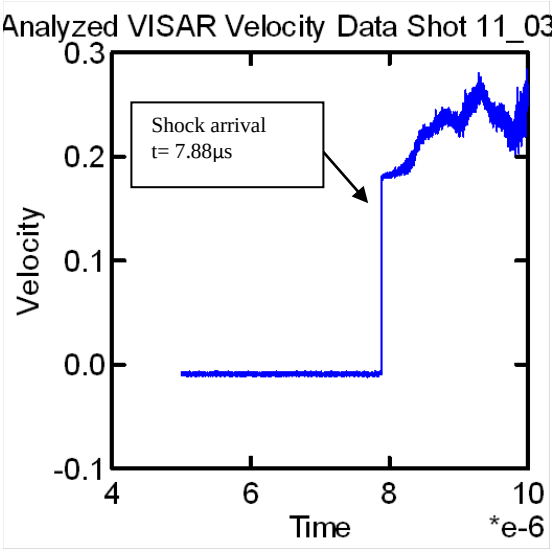

Figure 44. Analyzed VISAR velocity data for NPS shot 11_03

The pre-shot data for NPS shot 11_03 is listed in Table 2. From the VISAR data above and the data from Table 2, analysis of the shot was conducted based on the methods discussed in Chapter II. The analytical results of NPS shot 11_03 are listed in Table 3.

Table 2. Final experimental parameters for NPS shot 11_03

Shot Number	Impactor Thickness (mm)	Base Plate Thickness (mm)	Density of Cu (g/cc)	Measured C_L of Cu (mm/μs)	Target Thickness (mm)	Target Density (g/cc)	Expected Projectile Velocity (mm/μs)
11_03	8.017	3.996	8.924[5]	4.80	4.27	1.536	0.264

Table 3. Final analysis of data from NPS shot 11_03

Shot Number	Measured Projectile Velocity (mm/μs)	Measured Shock Arrival Time (μs)	Calculated Shock Velocity of Technical Sand (mm/μs)	Calculated Particle Velocity of Technical Sand (mm/μs)	Calculated Stress of Technical Sand (GPa)
11_03	0.267 ± 0.001	3.089	1.382±1.6%	0.2525±1.3%	0.536

The calculated shock velocity in the technical sand was much higher than originally expected. The original estimate of 0.80 was based on the work of Brown [3] et al. and his work on the shock response of dry sand done at Sandia National Laboratories due to the similarities between the technical sand and the sand used in their work. From the above data a final x-t diagram was constructed and is shown in Figure 45.

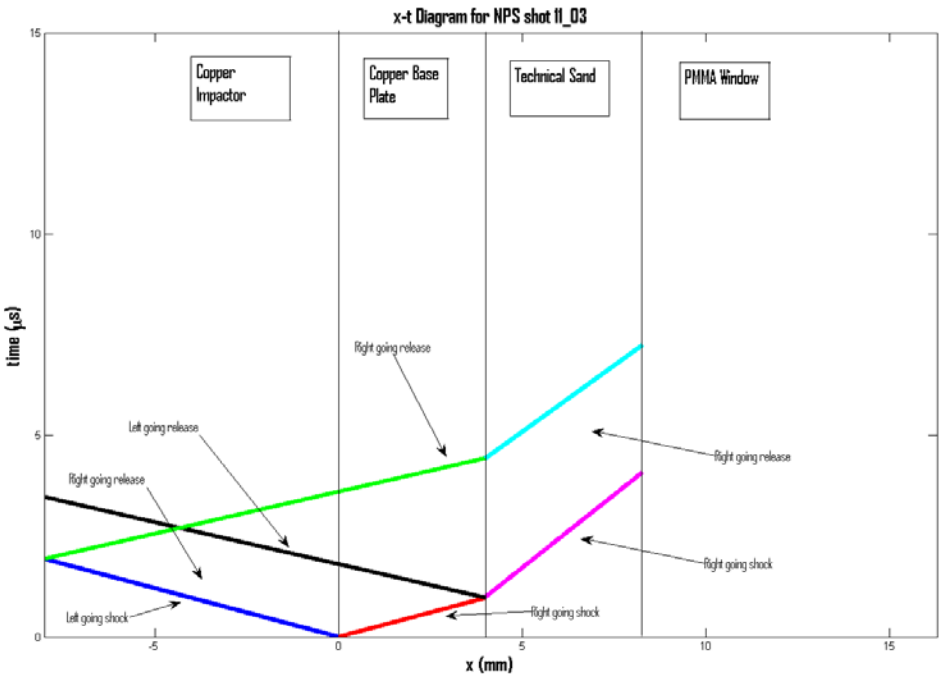

Figure 45. Final x-t diagram of NPS shot 11_03

2. NPS Shot 11_05

For shot 11_05 the same basic shot design was kept with the only difference being the reduced thicknesses of the copper impactor and copper base plate to four millimeters and two millimeters respectively. The goal of this shot was to try to match the data from shot 11_03 to ensure that the results were repeatable and to establish a first point on the Hugoniot. In order to anticipate the results of the experiment, a rough hand calculation was again performed using assumptions to predict the expected results. Again, a copper to copper symmetric impact was used allowing for simpler calculations at the interface

between the copper base plate and the technical sand. Using known Hugoniot data as found in Marsh [5] and data from Brown [3] et al., a desired projectile velocity of 0.264 mm/μs, and approximating the velocity of the longitudinal sound speed through the sand to be 1.43 mm/μs, an approximate x-t diagram was constructed to represent the anticipated results as shown in Figure 46.

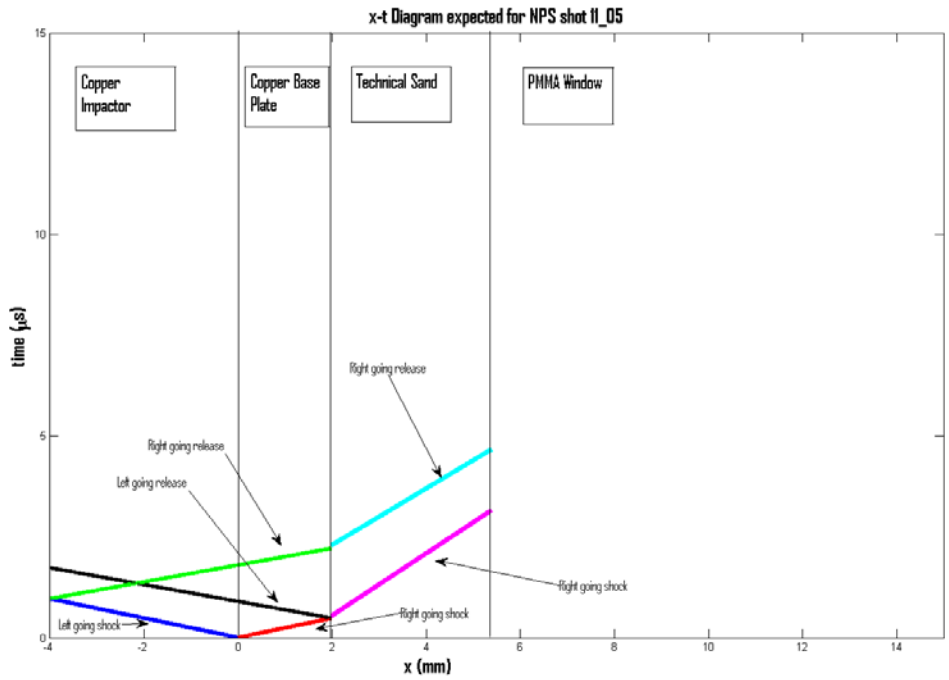

Figure 46. Preliminary x-t diagram for NPS shot 11_05

The anticipated arrival time of the shock wave at the target-window interface was 2.938 μs after impact and the expected arrival of the release at the target-window interface was 1.515 μs later. Using the measured diameter for the sand the releases were expected to pinch off through the wave at 6.837 μs after impact, which was well after the completion of the desired event of interest. For this shot, the shock arriving from the side arrived 4.071 μs after the event of interest occurred.

To achieve the projectile velocity of 0.280 mm/μs, using a projectile mass of 536.5 grams, the breech pressure that was required was 850 psi. The final dimensions of the copper impactor were 60.00 mm in diameter and 4.015 mm in thickness. For the

copper base plate they were 50.01 mm in diameter and 1.987 mm in thickness. The final dimensions of the technical sand were 41.83 mm in diameter and 3.394 mm in thickness.

The shot was successful. All flush pins and velocity pins triggered as expected providing good signal for projectile velocity, projectile tilt and a time fiducial marking the time of shock arrival at the copper base plate and technical sand interface. Usable VISAR data was obtained from the diagnostics that allowed for calculation of shock arrival time at the technical sand and PMMA window interface. However, once again, the intensity of the VISAR rapidly dropped off after impact not allowing for sufficient data collection to determine what occurred after the arrival of the shock at the interface. The VISAR intensity record is shown in Figure 47.

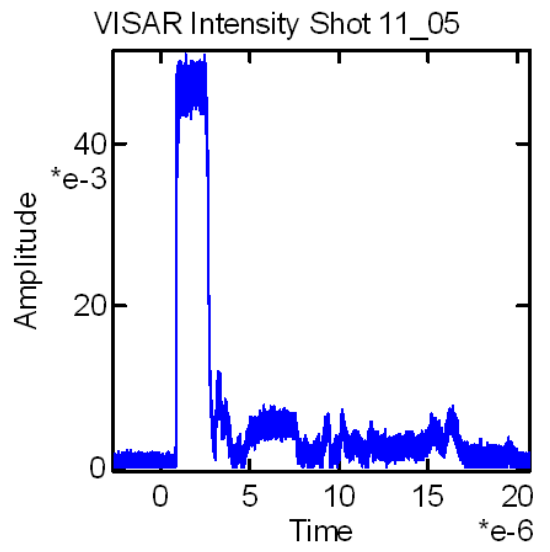

Figure 47. VISAR Intensity for NPS shot 11_05

A lost fringe was accounted for at the time of the loss of intensity, 2.517 μs, and the analyzed VISAR record is as shown in Figure 48.

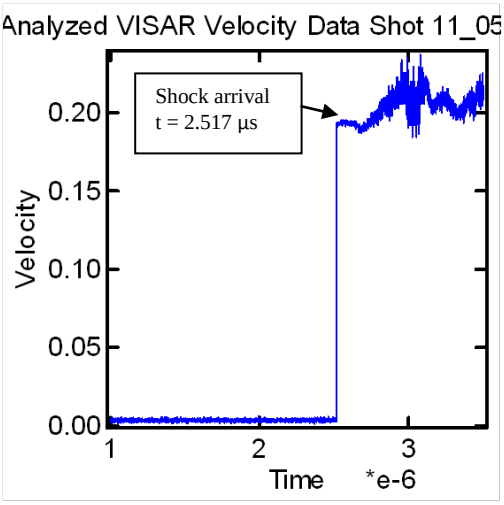

Figure 48. Analyzed VISAR velocity data for NPS shot 11_05

The pre-shot data for NPS shot 11_05 is listed in Table 4. From the VISAR data above and the data from Table 4, analysis of the shot was conducted based on the methods discussed in Chapter II. The analytical results of NPS shot 11_05 are listed in Table 5.

Table 4. Final experimental parameters for NPS shot 11_05

Shot Number	Impactor Thickness (mm)	Base Plate Thickness (mm)	Density of Cu (g/cc)	Measured C_L of Cu (mm/µs)	Target Thickness (mm)	Target Density (g/cc)	Expected Projectile Velocity (mm/µs)
11_05	4.015	1.987	8.924[5]	4.80	3.394	1.536	0.280

Table 5. Final analysis of data from NPS shot 11_05

Shot Number	Measured Projectile Velocity (mm/µs)	Measured Shock Arrival Time (µs)	Calculated Shock Velocity of Technical Sand (mm/µs)	Calculated Particle Velocity of Technical Sand (mm/µs)	Calculated Stress of Technical Sand (GPa)
11_05	0.288 ± 0.010	2.539	1.337±2.0%	0.2729±1.0%	0.5604

This data is in good agreement with shot 11_03. The shock velocity, particle velocity and pressure are all in the same regime. This shows that the results of this experiment are repeatable and allows for the establishment of a first point on the Hugoniot for technical sand in the low-pressure regime. A final x-t diagram of shot 11_05 is provided in Figure 49.

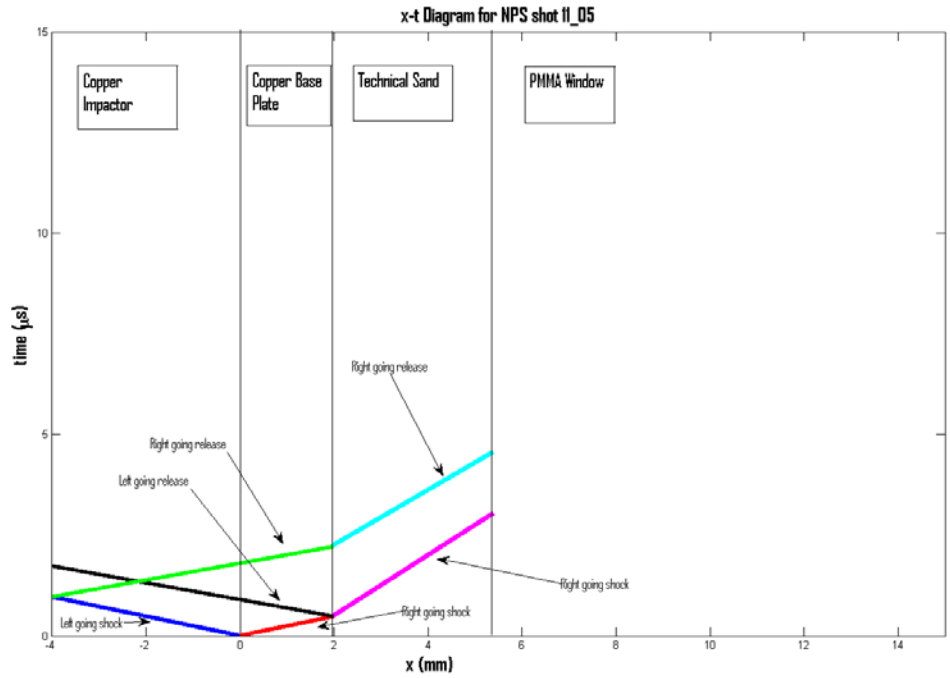

Figure 49. Final x-t diagram of NPS shot 11_05

3. NPS Shot 11_06

Shot 11_06 followed the same design patterns as shot 11_05. The goal of this shot was to try to obtain a shock velocity of 0.80 mm/μs as was originally attempted in shot 11_03. A desired projectile velocity of 0.168 mm/μs was selected and the expected x-t diagram for shot 11_06 is shown in Figure 50.

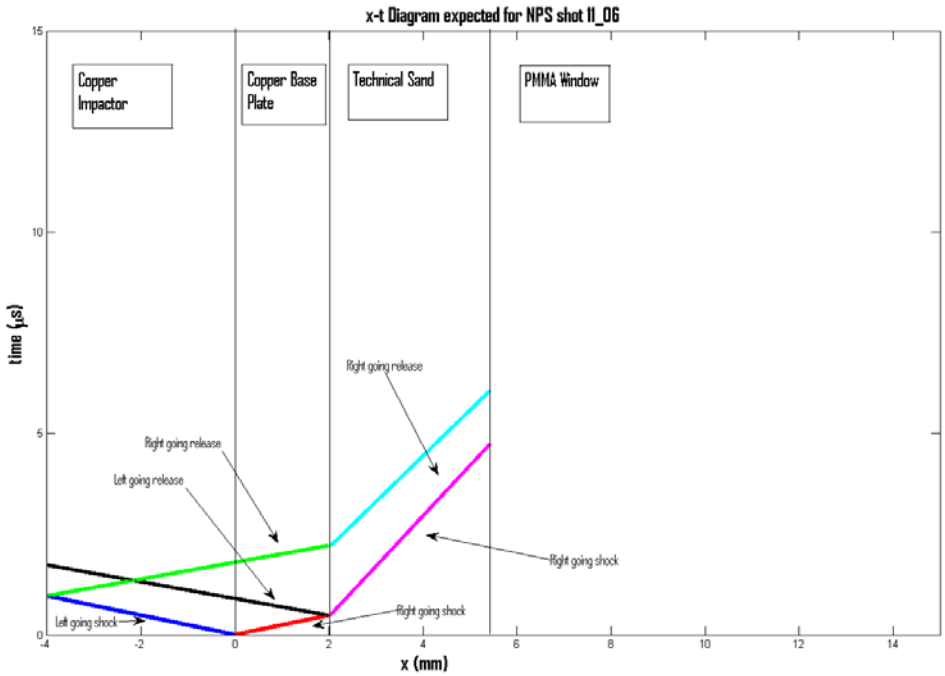

Figure 50. Preliminary x-t diagram for NPS shot 11_06

The anticipated arrival time of the shock wave at the target-window interface was 4.253 μs after impact and the expected arrival of the re-shock at the target-window interface was 1.856 μs later. Using the measured diameter for the target sample, the releases were expected to pinch off through the wave at 8.077 μs after impact.

To achieve the desired projectile velocity of 0.168 mm/μs, using a projectile mass of 528.1 grams, the breech pressure that was required was 300 psi. The final dimensions of the copper impactor were 59.99 mm in diameter and 4.004 mm in thickness. For the copper base plate, they were 50.00 mm in diameter and 2.025 mm in thickness. The final dimensions of the technical sand were 41.85 mm in diameter and 3.404 mm in thickness.

The shot was successful. All flush pins and velocity pins triggered as expected providing good signal for projectile velocity, projectile tilt and a time fiducial marking the time of shock arrival at the copper base plate and technical sand interface. Usable VISAR data was obtained from the diagnostics that allowed for calculation of shock arrival time at the technical sand and PMMA window interface. The intensity of the

VISAR rapidly dropped off after impact not allowing for sufficient data collection to determine what occurred after the arrival of the shock at the interface. A lost fringe was accounted for at the time of the loss of intensity, at 4.356 μs

This loss of intensity was addressed in shot 11_07 and will need additional shot data and analysis to resolve. It is believed that the intensity drops immediately after shock arrival due to the technical sand perforating the thin foil. The foil being used for the purpose of this research was a stainless steel shim of 0.013 mm thickness. It is believed that future shots should use a thicker foil and ensure that the foil is glued to the face of the PMMA window creating a tight bond and increased resistance to perforation. Shot 11_07 will use a copper back plate as a buffer for proof of concept that the loss of intensity can be prevented with adaptations to the experimental setup.

The pre-shot data for NPS shot 11_06 is listed in Table 6. From the VISAR data and the data from Table 4, analysis of the shot was conducted based on the methods discussed in Chapter II. The analytical results of NPS shot 11_06 are listed in Table 7.

Table 6. Final experimental parameters for NPS shot 11_06

Shot Number	Impactor Thickness (mm)	Base Plate Thickness (mm)	Density of Cu (g/cc)	Measured C_L of Cu (mm/μs)	Target Thickness (mm)	Target Density (g/cc)	Expected Projectile Velocity (mm/μs)
11_06	4.004	2.025	8.924[5]	4.80	3.404	1.536	0.168

Table 7. Final analysis of data from NPS shot 11_06

Shot Number	Measured Projectile Velocity (mm/μs)	Measured Shock Arrival Time (μs)	Calculated Shock Velocity of Technical Sand (mm/μs)	Calculated Particle Velocity of Technical Sand (mm/μs)	Calculated Stress of Technical Sand (GPa)
11_06	0.172 ± 0.001	3.402	1.001±1.2%	0.1647±1.1%	0.253

The expected shock velocity of 0.80 mm/μs was still not obtained there was success in lowering the shock velocity. The final x-t diagram for shot 11_06 is shown in Figure 51.

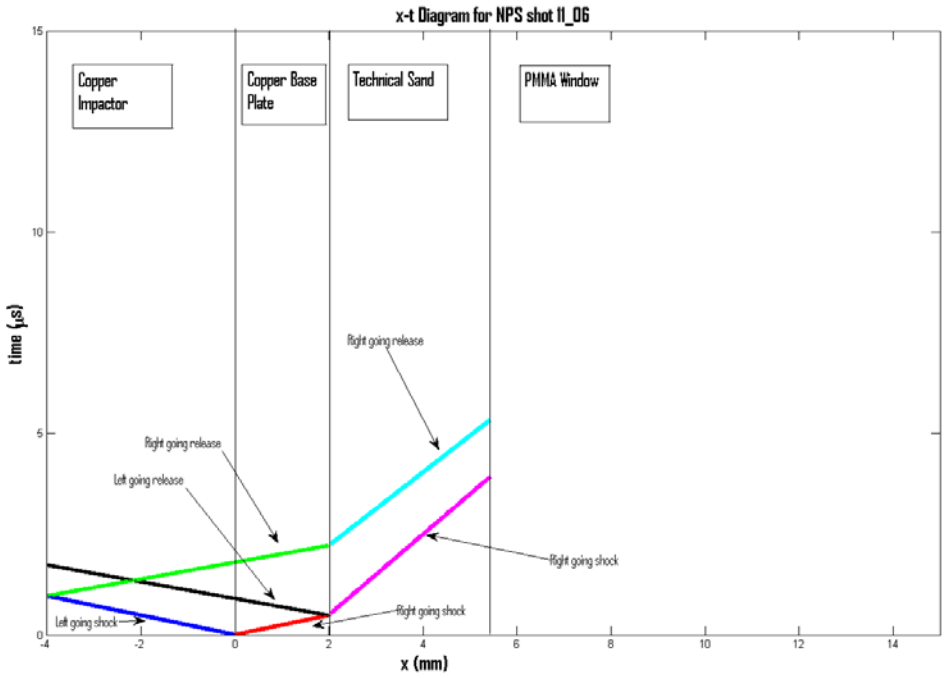

Figure 51. Final x-t diagram for NPS shot 11_06

4. NPS Shot 11_07

Shot 11_07 was modified to add a copper buffer between the technical sand and the PMMA window in order to prevent the loss of VISAR intensity upon arrival of the shock at the rear of the technical sand. The copper buffer was non-annealed OFHC copper of 18.94 mm diameter and 1.679 mm thickness. The copper buffer was glued to the PMMA window in order to provide a close bond. The copper was also polished on the PMMA window side in order to allow for good reflectivity of the VISAR and ensure good data collection. The goal of this shot is maintain VISAR intensity throughout and to try to get in the same regime as shots 11_03 and 11_05.

Using this redesign in target assembly caused an adjustment in the methods of analyzing the data that was recorded. The experiment is no longer a traditional shock Hugoniot experiment but is rather more analogous to a 'plate push' experiment. Multiple wave interactions will occur throughout the duration of the experiment and through the five different layers of material. The only waves that are of interest however, are the waves that travel through the technical sand sample and the copper back plate. This is because the reference time for the shock entering the front face of the technical sand is directly measured by the two PZT pins in contact with the copper base plate.

The waves in the copper back plate will be of importance to ensure that the experimentalist understands the results obtained from the VISAR record trace. When the shock wave travelling through the copper back plate reaches the window, the shock will be reflected back as a release wave travelling back to the technical sand and copper back plate interface. When the release reaches this interface it will be reflected back into the copper back plate as a re-shock until it reaches the window. This process of release and re-shock will continue to occur, continually stepping up the particle velocity seen on the VISAR record up to a max value.

The arrivals of the shock wave in the copper back plate should also correspond to times of a round trip shockwave in the buffer material. These interactions and the expected results of this shot are shown in the x-t diagram in Figure 52. Note that for the purposes of this research, only the arrival of the first shock through the copper back plate was needed and measured. This arrival time was used to help calculate the shock speed in the sand.

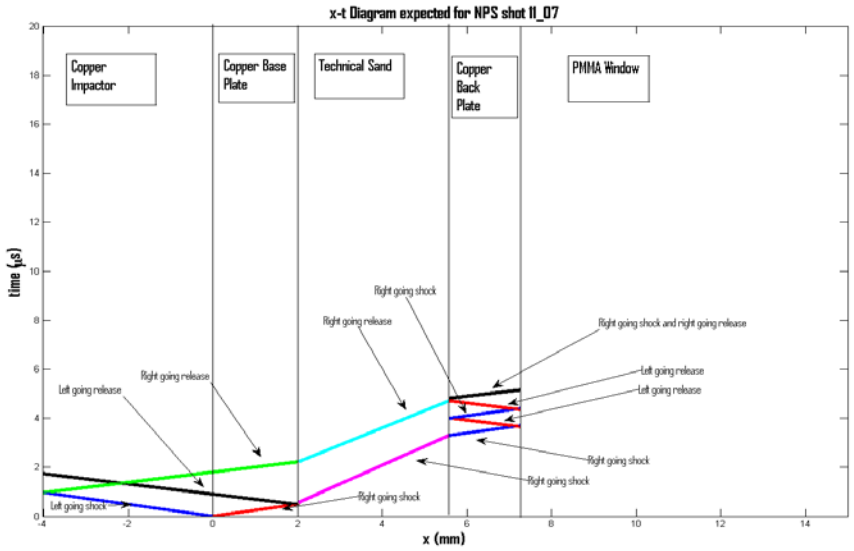

Figure 52. Preliminary x-t diagram for NPS shot 11_07

The shot was successful. All flush pins and velocity pins triggered as expected providing good signal for projectile velocity, projectile tilt and a time fiducial marking the time of shock arrival at the copper base plate and technical sand interface. Usable VISAR data was obtained from the diagnostics that allowed for calculation of shock arrival time at the rear of the copper back plate and PMMA window interface. VISAR intensity was maintained throughout the duration of the experiment as shown in Figure 53.

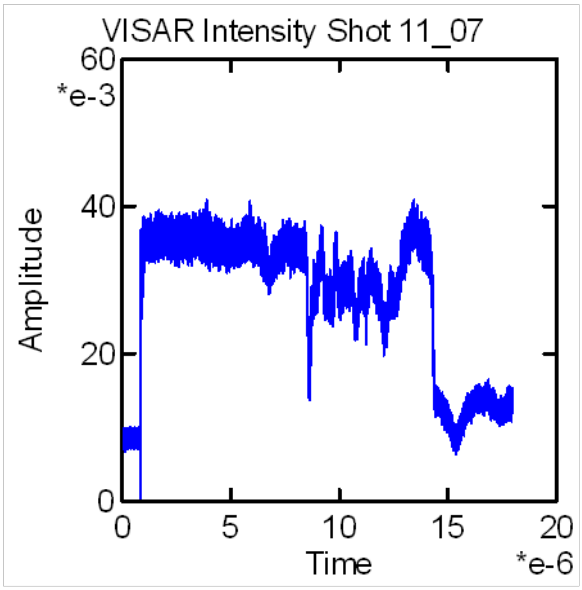

Figure 53. VISAR intensity for NPS shot 11_07

A good VISAR velocity trace was obtained from the copper back plate. The VISAR trace showed an initial rise to a small plateau correlating to the Hugoniot state in the technical sand. A subsequent ring-up was observed although not as clearly stepped as expected. However, a better defined ring-up in the copper back plate was noticed at two points. This is believed to be due to the arrival of release waves at the rear of the interface at the same time as the re-shocks through the copper back plate are arriving. The VISAR velocity data is shown in Figure 54.

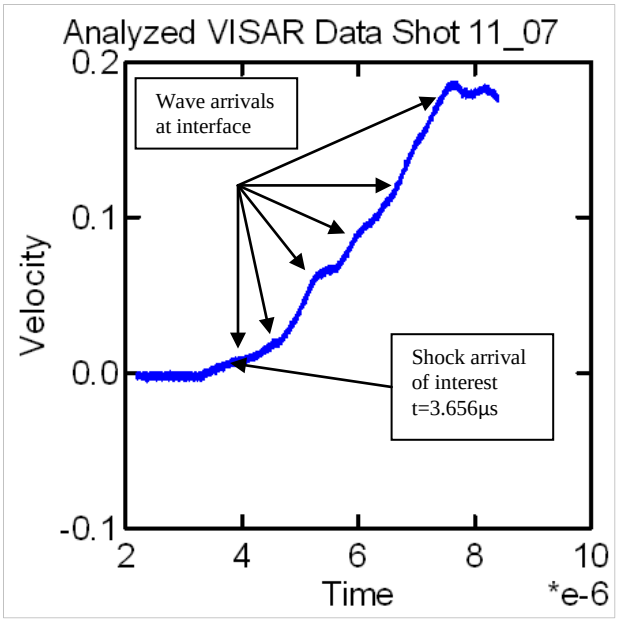

Figure 54. Analyzed VISAR date for NPS shot 11_07

In order to calculate the shock velocity in the technical sand, the shock velocity at the rear of the copper back plate needs to be calculated. Taking the VISAR velocity indicated by the VISAR trace at the window interface gives the particle velocity behind the shock in the copper back plate. Using the known copper Hugoniot data from Marsh [5], the shock velocity in the copper back plate was calculated. This shock velocity was then used to determine the time required for the shock to transit through the copper back plate. This time was then subtracted from the time indicated in Figure 54 to find the shock arrival time at the technical sand-copper back plate interface. Using the reference arrival time measured by the PZT pins, and this calculated time, the shock speed in the technical sand was calculated using the previously discussed simple velocity relationship.

The particle velocity of the technical sand is then calculated through the method of impedance matching discussed in Chapter II. The pre-shot data for NPS shot 11_07 is listed in Table 8. From the VISAR data and the data from Table 8, analysis of the shot was conducted. The analytical results of NPS shot 11_07 are listed in Table 9 and the final x-t diagram is shown in Figure 55.

Table 8. Final experimental parameters for NPS shot 11_07

Shot Number	Impactor Thickness (mm)	Base Plate Thickness (mm)	Density of Cu (g/cc)	Measured C_L of Cu (mm/μs)	Target Thickness (mm)	Target Density (g/cc)
11_07	4.026	2.039	8.924[5]	4.79	3.552	1.361
	Expected Projectile Velocity (mm/μs)	Cu Back Plate Thickness (mm)	Measured C_L of Cu Back Plate (not annealed) (mm/μs)	Measured C_S of Cu Back Plate (not annealed) (mm/μs)		
	0.281	1.679	4.70	2.30		

Table 9. Final analysis of data for NPS shot 11_07

Shot Number	Measured Projectile Velocity (mm/μs)	Measured Shock Arrival Time (μs)	Calculated Shock Velocity of Technical Sand (mm/μs)	Calculated Particle Velocity of Technical Sand (mm/μs)	Calculated Stress of Technical Sand (GPa)
11_07	0.2835 ± 0.0002	2.403	1.478±4.2%	0.2903±4.2%	0.5840

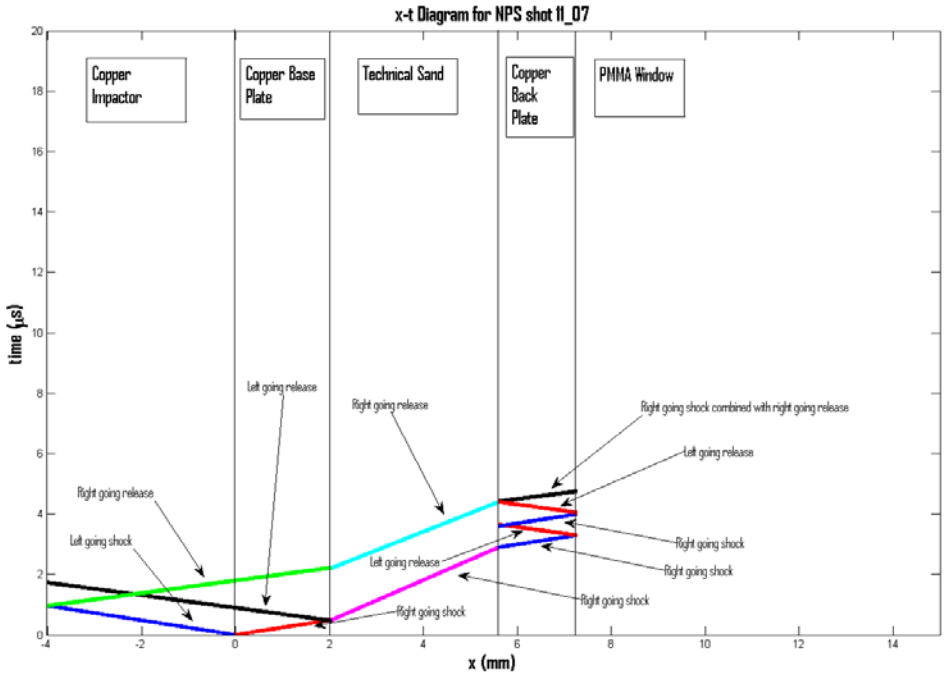

Figure 55. Final x-t diagram for NPS shot 11_07

There is good correlation between the expected results and the measured experimental results.

B. SHOCK HUGONIOT MEASUREMENT OF TECHNICAL SAND UNCERTAINTY ANALYSIS

Significant errors were noticed when measuring the ambient density of the technical sand and the Hugoniot stress. The primary reason for this high uncertainty error for the ambient density is due to the lack of a high precision balance able to measure the mass of the samples out to several decimal places. Given the formal uncertainty analysis method, a larger uncertainty than expected is incorporated into the calculation. It is believed that this calculated uncertainty is significantly higher than the actual uncertainty due to this reason. An additional reason for the error in the ambient density measurement may be related target design and construction. The barrel assembly consists of multiple parts that must be screwed and glued together in order to contain the technical sand. Any error in the assembly process is likely to carry over and affect the

measured density of the sand. For example, if the window were slightly canted to one side then it would allow for a very small gap between portions of the technical sand and window. However, this error would be significantly smaller than the error due to the lack of a high precision balance.

This uncertainty carries over to the Hugoniot stress state, as it is directly dependent on the ambient density of the target sample. Following the analysis set forth in Chapter II of this research, the percent error in measured ambient density, shock velocity, particle velocity and stress level were calculated and summarized in Table 10.

Table 10. Summary of percent error for technical sand measurements

Shot Number	Percent Error in Ambient Density	Percent Error in Shock Velocity	Percent Error in Particle Velocity	Percent Error in Stress
11_03	19.7%	1.6%	1.3%	21.6%
11_05	15.6%	2.0%	1.0%	15.8%
11_06	15.7%	1.5%	1.1%	15.8%
11_07	18.4%	4.2%	4.2%	19.3%

C. LOW PRESSURE U_S-u_p AND P-u_p

This research has successfully determined the first points on the Hugoniot for this technical sand in the low-pressure regime below one GPa. For comparison, between the technical sand and an actual sand sample, the results from Brown [3] et al. at Sandia National Labs that falls into the same pressure regime has been included in Table 11 and on the plots of the U_S-u_p and P-u_p diagrams shown in Figure 56 and Figure 57. There is a good linear relationship between the data points with a U_S-u_p relationship of: $U_S = 0.414 + 3.612u_p$.

Table 11. U_S-u_p and P-u_p data comparison from NPS and Sandia

NPS Data			Sandia Data		
u_p (mm/μs)	U_S (mm/μs)	P (GPa)	u_p (mm/μs)	U_S (mm/μs)	P (GPa)
0.1647	1.001	0.253	0.24	0.79	0.29
0.2525	1.382	0.5360	0.23	0.80	0.29
0.2729	1.337	0.5604	0.43	1.31	0.88
0.2903	1.478	0.584	0.44	1.21	0.82

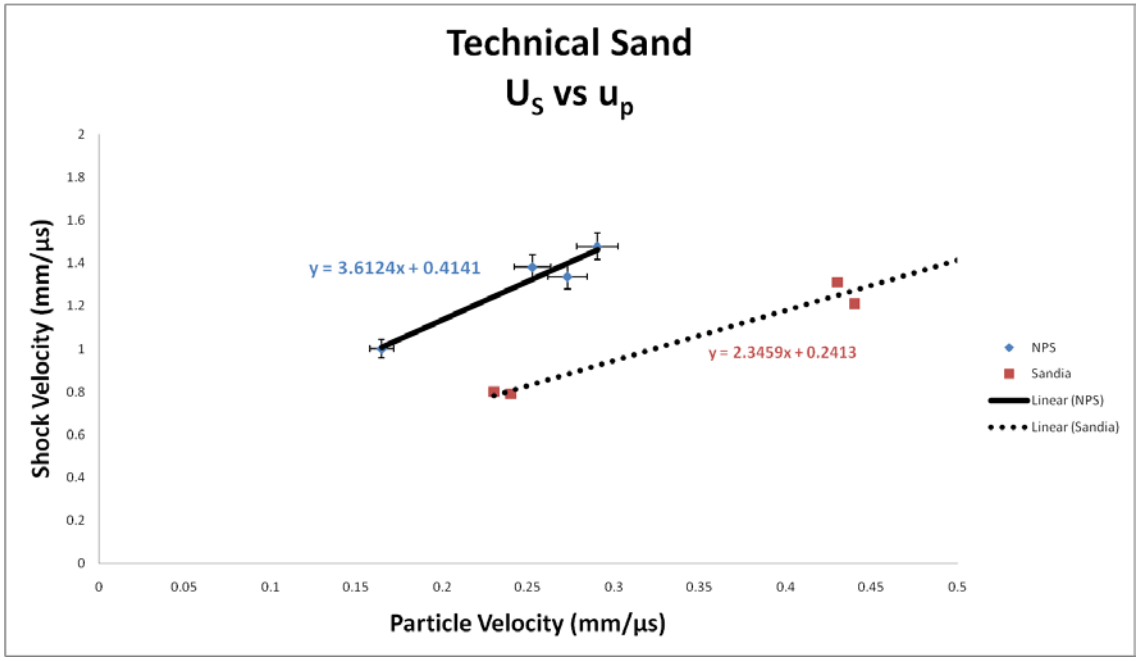

Figure 56. U_S-u_p relationship for technical sand in low pressure regime

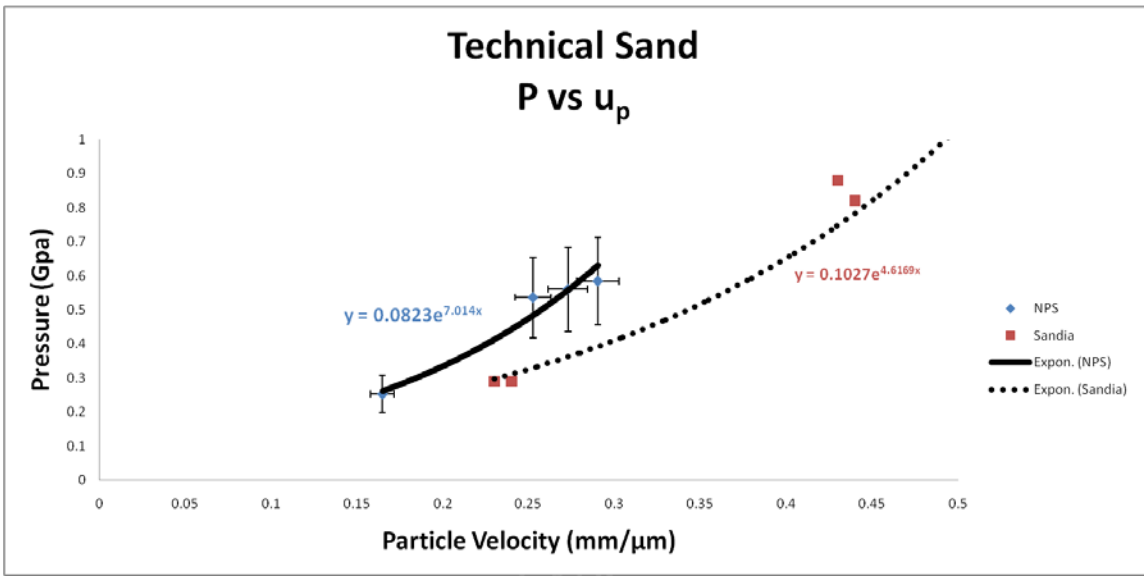

Figure 57. P-u_p relationship for technical sand in low pressure regime

IV. CONCLUSION

A. BRIEF SYNOPSIS OF ACHIEVEMENTS

This research successfully established and developed the experimental setup and procedure for experimentation with porous and granular materials at the Naval Postgraduate School Impact Physics Laboratory. This allowed for the successful measurement of the first several data points for the technical sand in the low-pressure regime below one GPa. Based on the results of these measurements and their comparison to data collected on actual sand samples, it has been shown that this technical sand is a viable alternative for the modeling of sand. This will allow for a standardized material reference to be used in future research and will allow for the repetition of experiments along with better correlation and comparison of data independent of geographic location. This will greatly help in the continued study of sand and in developing an increased understanding of its dynamic response.

B. FOLLOW-ON RESEARCH

Additional research is needed to verify the recommendations made for improvement of data collection and the experimental setup. In order to reduce the experimental error found in the ambient density measurements and the stress state measurements, a more precise balance will need to be procured for use in the pre-experiment data collection process. The use of a thicker piece of foil glued to the face of the PMMA window that would reduce or stop the loss of the VISAR intensity from perforation by the technical sand needs to be examined. Additionally, a new design of barrel assembly is recommended that would combine the window and barrel into a single piece of fabricated PMMA with a fixed sample depth of 3.5 mm, which was determined to be the optimum sample thickness for experimentation with sand.

Follow-on research is needed to fully characterize the Hugoniot for the technical sand throughout all pressure regimes. Upon the successful characterization of the Hugoniot, material models for use in hydro-codes will need to be created for future modeling and simulation purposes.

APPENDIX A – SHOT PREPARATION CHECK LIST

SHOT PROCEDURE

SHOT # _____ Date Started _____

Date Completed _____

I. Initial Data Collection

A. Anneal copper impactor and anvil in annealing ovens at 350 °C for 4 hrs

B. Lap copper impactor and anvil to within ± 0.005 mm

C. Complete the tables below:

IMPACTOR	Mass (g)	Thickness (mm)	Diameter (mm)	Sound Speed Times (μs)	Sound Speed (km/s)

ANVIL	Mass (g)	Thickness (mm)	Diameter (mm)	Sound Speed Times (μs)	Sound Speed (km/s)

	Bullet	Constructed Bullet	Barrel	Constructed Barrel	PMMA Window	Target Plate
Mass (g)						
Thickness/Height (mm)						
Diameter (mm)				Inner: Outer:		

II. Bullet Preparation

A. Select bullet type based on desired impact velocity

B. Bore out inset into nose of bullet to hold the impactor. Ensure that there is a step from the bottom of the inset for the impactor to rest on.

C. Drill out small a half circle notch on the edge of the inset that goes to the bottom of the inset in order to allow any air to escape when placed under vacuum.

D. Apply angstrom bond to bottom and sides of inset leaving ~ 20° of clear surface around the notch to ensure that air has unobstructed path to escape through

E. Insert impactor into inset and apply even pressure. Let cure for at least 18 hours.

F. Face the constructed bullet

G. Measure the mass of the constructed bullet

H. Measure and record the flushness of the impactor relative to the bullet face

Average protrusion or recession of impactor relative to bullet face:
+: for protrusion
-: for recession
x_{imp} = _____

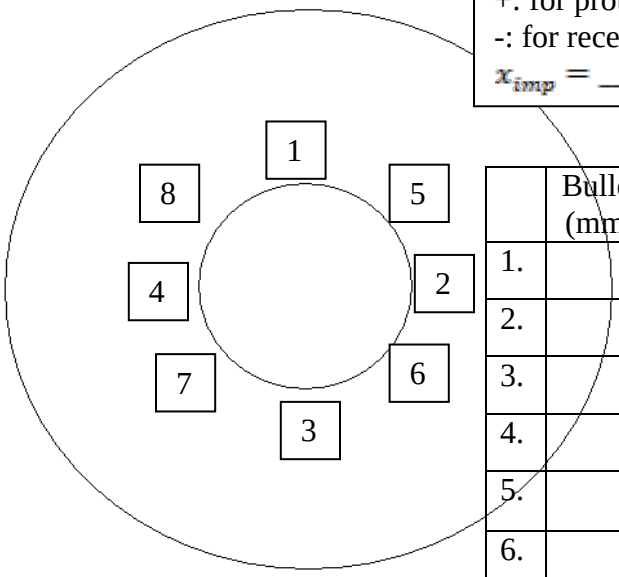

	Bullet (mm)	Impactor (mm)	Difference (mm)
1.			
2.			
3.			
4.			
5.			
6.			
7.			
8.			

III. Target Preparation

A. Target Plate

1. Bore out center of target plate to hold barrel assembly

2. Bore out velocity pins holes in target plate and record velocity pin radius: _____

3. Lap impact side of target plate

B. Barrel Assembly

1. Attach copper anvil to barrel
2. Measure the mass of the constructed barrel

C. Use gluing fixture to glue barrel assembly to target plate with epoxy and let cure for at least 2 hrs

D. Glue velocity pins to required heights using epoxy and let cure for 2 hrs

VP1	2 mm
VP2	4 mm
VP3	6 mm
VP4	8 mm
VP5	10 mm
VP6	12 mm
GND	14 mm

E. Measure and record velocity pin exact heights

Pin #	1	2	3	4	AVG
VP1					
VP2					
VP3					
VP4					
VP5					
VP6					
GND					

F. Measure the mass of the barrel and target plate assembly _____

G. Fill barrel with desired amount of technical sand and record its thickness

H. Measure the mass of the filled barrel and target plate assembly _____

I. Glue reflective material to sample side of the PMMA window (if necessary) using angstrom bond, let cure at least 18 hrs

J. Insert PMMA window into the barrel

K. Check VISAR reflectivity on the sample

L. Compress technical sand to desired pressure and record the pressure applied and the length of time it was applied: Pressure ___ time _____

M. Measure and record PMMA window height after compaction _____

N. Allow time for sand to rebound and measure window height and rebound time:

	Height (mm)	Height Calculation	Time
1.		$H_{SAND} = H_{avg} - H_{PMMA} - H_{ANVIL}$	
2.			
3.		$H_{SAND} =$	
4.			
5			
AVG			

O. Glue PMMA window into place using epoxy and let cure for 2 hrs
P. Calculate density of sand in barrel assembly

_____

Q. Solder velocity pin wires to velocity pins
R. Test flush and trigger pins using the O-Scope, replace if necessary
S. Solder flush pin and trigger pin cables to pins
T. Glue flush pins into barrel assembly and let cure for 2 hrs
U. Glue trigger pin so that it is flush with the anvil face
V. Attach VISAR probe holder to target plate
W. Mount target plate to Gun
X. Attach BNC cables and velocity pin connector to appropriate connectors
Y. Insert VISAR probe and tune VISAR and record required power for the shot _____

IV. Gun Firing Procedure
A. Use Gun Firing Procedure Appendix

V. Post Shot Analysis
A. Transfer raw data from laptop to flash drive for analysis in test1.exe program
B. Tilt calculation
1. Record arrival time of each velocity pin

	VP1	VP2	VP3	VP4	VP5	VP6	GND
Raw Time							

2. Use tilt program to calculate and record the tilt _____
3. Experimental U_D _____

C. Calculate the shock velocity
1. Record raw time of arrival for FP1 _____ and FP2 _____
2. Take average of time arrival for flush pins $T_{FP\ avg}$ = _____
3. Record raw time of onset of elastic wave profile T_e = _____
4. Subtract $T_{FP\ avg}$ from T_e to get ΔT_{RAW}
$\Delta T_{RAW} = T_e - T_{FP\ avg}$ = _____
5. Calculate shock velocity (U_s): $U_s = x_{sand} / \Delta T_{RAW}$ = _____
6. Calculate the u_p of the Cu: $u_{p\ Cu} = ½ * U_D$ = _____
7. Calculate the U_s of the Cu: $U_s = C_0 + (s * u_p)$ = _____
8. Calculate the impedance of the sand: $Z_{SAND} = \rho_{0\ SAND} * U_{S\ SAND}$ = _____

9. Calculate the impedance of the Cu: $Z_{Cu}=\rho_{0\ Cu} * U_{S\ Cu}$ = _____

10. Calculate the u_p of the sand:
$u_{p\ SAND} = u_{p\ Cu} * (\rho_{0\ Cu} / \rho_{0\ SAND}) * (U_{S\ Cu} / U_{S\ SAND}) * ((2 * Z_{SAND}) / (Z_{SAND} + Z_{Cu})$ = _____

11. Calculate the Pressure: $P_{SAND} = \rho_{0\ SAND} * U_{S\ SAND} * u_{p\ SAND}$ = _____

THIS PAGE INTENTIONALLY LEFT BLANK

APPENDIX B – GAS GUN OPERATING PROCEDURE

LOW PRESSURE GAS GUN STANDARD OPERATING PROCEDURES

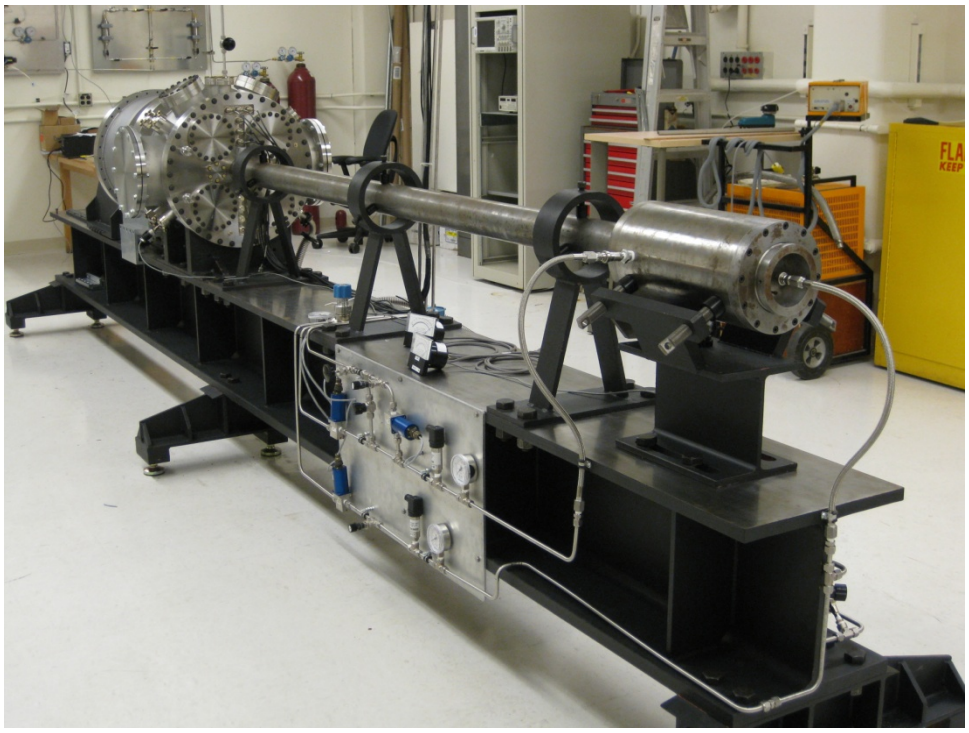

IMPACT PHYSICS LABORATORY

NAVAL POSTGRADUATE SCHOOL

Monterey, CA

Preface

All procedures contained herein will be performed by no more than two persons operating under restrictions of reader-worker routine. Reader-worker routine is defined as: One person (preferably the senior member) reading the procedure and keeping track of status of steps of the procedure while a second person performs steps of the procedure as directed by the reader.

WARNINGS, CAUTIONS AND NOTES

1. Update all valve manipulations as they occur on system status board.
2. During Firing procedure only authorized personnel are allowed in the Impact Physics Lab(IPL). This will be limited to Professors and students directly associated with the IPL and any specifically authorized visitors cleared by the head of the IPL.
3. During performance of the procedures contained herein, workers are not to engage in outside conversation and are to discourage outside distractions from any other parties.

Gun Evacuation Procedure

1. Ensure gun barrel is fully seated.
2. Verify gun barrel and catch tank clear of debris
3. Verify target installed and diagnostics connected per target preparation and installation procedure
4. Install honeycomb and momentum absorbers in catch tank
5. Clean catch tank o-ring mating surfaces and apply fresh vacuum grease
6. Close catch tank to furthest point possible by hand
7. Apply vacuum grease to projectile o-rings
8. Install o-rings on projectile and wipe excess grease from projectile surfaces
9. Insert projectile into projectile cavity until projectile is fully inserted into breech
10. Install breech plug
11. Install breech screw cap
12. Connect vacuum hose between SV-1 and breech plug
13. Shut SE-1, SE-5
14. Check shut SE-3, SP-1, SP-2, SV-1, SV-2
15. Shut catch tank vent plugs, being careful not to pinch o rings
16. Verify VISAR probe bolt plug installed and filled with hardened epoxy on top of catch tank
17. Shut vacuum pump suction valve
18. Energize vacuum pump
19. Open SV-1 wait 30 seconds
20. Open SV-2
21. Slowly adjust vacuum pump suction valve to throttle position that corresponds to optimum operation
22. Move catch tank shock absorber forward when catch tank is fully seated and insert stop bolts and stop pins
23. When breech and catch tank press ≈500mtorr check for system leaks as follows:
    a. Open He bottle isolation valve
    b. Open SP-4 and SP-5 regulator isolation valves
    c. Adjust SP-5 to 1200psig
    d. Adjust SP-4 to 200psig
    e. Stand clear of pressure indication panel

f. Open SP-1
g. Verify system vacuum holding steady
h. Shut SP-1
i. If indication of failed projectile o-rings, depressurize and remove projectile as follows
    i. Shut SV-2
    ii. Shut SV-1
    iii. De-energize vacuum pump
    iv. Open SE-5 and allow catch tank to equalize with atmosphere
    v. Open SE-3 to vent breech to atmosphere
    vi. When local breech pressure indication reads 0 psig, remove breech screw cap
    vii. ***CAUTION: DO NOT STAND DIRECTLY BEHIND BREACH DO TO THE POSSIBILITY OF A REAR FIRING OF THE PROJECTILE IF PLUG IS SEPARATED FROM BULLET WHILE REMOVING FROM BREECH.***

    Carefully remove breech plug with vacuum hose attached. Projectile should be vacuum sealed to breech plug
    viii. Carefully remove projectile from breech plug and inspect o-rings for damage
    ix. Replace projectile o-rings and vacuum grease if necessary
    x. Repair any other known leaks in system
    xi. Open catch tank and inspect target integrity if necessary
    xii. Return to step 8.

24. Continue evacuating Projectile Cavity and Catch tank until vacuum indicates ≤100mtorr on both breech and catch tank vacuum gauges(≤50mtorr preferred)
25. If gun is not to be shot immediately
    a. Shut SV-2
    b. Shut SV-1
    c. De-energize vacuum pump
26. Continue to Diagnostic Setup if gun is to be fired immediately

DIAGNOSTIC SETUP

1. Power up diagnostics laptop
2. Energize oscilloscope #1 and #2
3. Energize laser power
4. Energize velocity pin circuit
5. Adjust velocity pin circuit voltage to 120 to 150V
6. Setup VISAR system as follows
    a. Energize BNC pulse generator
    b. Energize frequency generator
    c. Energize high voltage power supply as follows:
        i. Depress power button
        ii. Wait 10 seconds
        iii. Depress high volts switch
7. Test diagnostics triggering properly as follows:
    a. Connect test piezoelectric pin cable to EXT/GATE connection on pulse generator
    b. On Function generator:
        i. Depress stop button
        ii. Depress FUNCTION button until setup appears on screen
        iii. Depress NEXT until RECALL appears on screen
        iv. Depress up or down arrow button until #4 appears on screen
        v. Depress FUNCTION until setup once again appears
        vi. Depress RUN button
    c. On diagnostics laptop:
        i. Open test1.py program
        ii. Enter current setup file name both9.txt
        iii. Type “arm” in command window
    d. Tap test piezoelectric pin
    e. Type “no” when prompted to save data on diagnostics laptop
    f. Press STOP on function generator
    g. Remove test cable from function generator and replace with Trigger Pin connector
    h. Turn off function generator
8. When ready to shoot:
    a. Type “arm” on diagnostics laptop
    b. Depress RUN on function generator

GUN FIRING PROCEDURE

1. Clear lab space of all unauthorized personnel
2. Verify completion of Gun Evacuation procedure
3. Verify completion of system diagnostic setup procedure
4. Verify catch tank shock absorber in the full forward position with stop pins and stop bolts installed
5. Check shut SP-1, SP-2, SE-3, SE-1, SE-5,
6. Check open SE-4, SV-1, SV-2
7. Verify vacuum pump energized
8. Verify SP-5 set to 1200psig
9. Adjust SP-4 to calculated firing pressure
10. Verify SP-6 set to ≈100psig
11. Verify all personnel clear of gun space and shut gun room doors
12. Shut and lock IPL door
13. Verify diagnostics armed and ready to receive data
14. Open SP-1 to charge breech
15. Shut SP-1 when calculated firing pressure is reached on remote breech pressure indication
16. Shut SV-2, SV-1
17. Ensure function generator is turned off
18. ***CAUTION: THIS WILL CAUSE THE PROJECTILE TO FIRE***
    To fire Gun: Cycle SP-2 open then shut to fire gun and record breech pressure at time of fire
19. Verify proper operation of diagnostics
20. Press enter to save and back up data from diagnostic equipment
21. De-energize vacuum pump
22. Shut He bottle isolation valve
23. Open SE-1 and SE-5 to equalize pressure in gun with atmospheric pressure
24. Open SP-1 to relief line pressure
25. Adjust SP-5, and SP-4 to fully counter clockwise position
26. Close SP-5 & SP-4 isolation valve after pressure relieved.
27. De-energize laser power
28. Open catch tank vent plugs
29. Remove Catch tank shock absorber stop bolts and stop pins
30. Open catch tank
31. Clear debris from catch tank
32. Remove vacuum hose from breech plug
33. Remove breech screw cap
34. Remove breech plug
35. Clean barrel
36. Verify data saved from diagnostics

37. De-energize diagnostics
38. Return barrel to fully inserted position

NOTES:

LIST OF REFERENCES

[1] Science@NASA. *Science News*. October 21, 2010. http://science.nasa.gov/science-news/science-at-nasa/2010/21oct_lcross2/ (accessed May 07, 2011).

[2] Soil Survey Division Staff. 1993. Soil Survey Manual. Soil Conservation Service. U.S. Department of Agriculture handbook 18.

[3] J. Brown et al., "Shock Response of Dry Sand," Sandia National Laboratories, Albuquerque, New Mexico, August 2007.

[4] W. Herrman, "Constitutive Equation For The Dynamic Compaction Of Ductile Porous Materials," Sandia Laboratories, Albuquerque, New Mexico, December 12, 1968. Reprinted from *Journal of Applied Physics*, vol. 40, no. 6, pp. 2490–2499, May 1969.

[5] S. P. Marsh, *LASL Shock Hugoniot Data*, University of California Press, 1980.

[6] L. Bennett, "CeO Powder with the Five Point VISAR," Los Alamos National Laboratories, Los Alamos, New Mexico, June 2004.

[7] W. F. Hemsing, "Velocity sensing Interferometer (VISAR) modification," *Review of Scientific Instruments*, vol. 50, no. 1, pp. 73–78, January 1979.

[8] C. C. Ho. "Assembly and Commissioning of Naval Postgraduate School gas gun for impact studies," M.S. thesis, Naval Postgraduate School, Monterey, CA, December 2009.

[9] J. R. Denzel, "Determination of Shock Properties of Ceramic Corbit 98: 98% Alumina," M. S. thesis, Naval Postgraduate School, Monterey, CA, June 2010.

[10] J. R. Garner, "Dynamic Material Properties of Orthotropic Polymer and Molybdenum for use in Next Generation Composite Armor Concept," M.S. thesis, Naval Postgraduate School, Monterey, CA May 2011.

THIS PAGE INTENTIONALLY LEFT BLANK

INITIAL DISTRIBUTION LIST

1. Defense Technical Information Center
   Ft. Belvoir, Virginia

2. Dudley Knox Library
   Naval Postgraduate School
   Monterey, California

3. Robert Hixson
   Los Alamos National Lab
   Los Alamos, New Mexico

4. Jose Sinibaldi
   Lawrence Livermore National Lab
   Livermore, California